Nanoscale

Accepted Manuscript

This article can be cited before page numbers have been issued, to do this please use: L. Liu, M. Zhang, N. Fang, L. Ding and Y. Chu, *Nanoscale*, 2025, DOI: 10.1039/D5NR01880C.

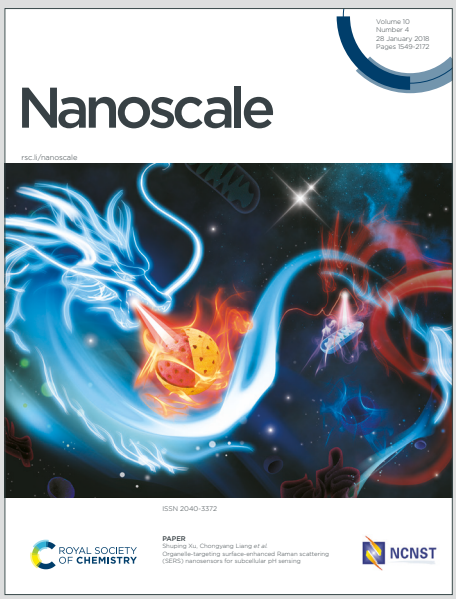

ROYAL SOCIETY OF CHEMISTRY

rsc.li/nanoscale

View Article Online
DOI: 10.1039/D5NR01880C

Effect of Perovskite Electronic Structure Modulation on Catalytic Combustion of VOCs

Liangyu Liu, Min Zhang, Ningjie Fang*, Ling Ding, Yinghao Chu*

College of Architecture and Environment, Sichuan University, Chengdu, Sichuan, China

***Corresponding author.**

E-mail address: fnj@scu.edu.cn (N. Fang); chuyinghao@scu.edu.cn

Abstract: The emission of volatile organic compounds (VOCs) is a serious threat to the environment and human health, and catalytic combustion technology has become an important direction for the treatment of VOCs due to its high efficiency and environmental friendliness. However, traditional catalysts suffer from insufficient low-temperature activity, poor stability, and weak anti-poisoning capability. Perovskite (ABO_3) materials have emerged as highly promising alternative catalysts due to their tunable electronic structure, abundant oxygen mobility, and flexible redox properties. In this paper, we systematically review the effects of the electronic structure of perovskites (e.g. cation defects, B-site elements, oxygen vacancies) on catalytic performance through modulation strategies such as doping modification (elemental substitution at A/B/O sites) and surface reconstruction (acid-base etching). In addition, this paper elucidates the relationship between specific electronic structure parameters (e.g., d-band center position, oxygen vacancy concentration, charge transfer barrier) and catalytic performance by resolving their enhancement mechanisms. These findings

View Article Online
DOI: 10.1039/D5NR01880C

provide comprehensive theoretical guidance and actionable technological pathways for developing efficient, stable, and adaptable catalytic materials for VOCs. Finally, machine learning-based high-throughput design, dynamic electronic structure resolution, and scale-up preparation techniques are envisioned to advance perovskite catalysts.

Keywords: Volatile organic compounds; Perovskite; Catalytic combustion; Electronic Structure

1. Introduction

Volatile organic compounds (VOCs) (including halogenated compounds, chlorinated hydrocarbons, sulfur-containing odor compounds, aldehydes, alcohols, ketones, aromatic compounds and ethers) emitted into the environment continue to increase with rapid urbanization and industrialization.[1,2] Owing to their relatively high vapor pressure under ambient conditions, VOCs readily evaporate and diffuse into the atmosphere. These toxic VOCs are produced both indirectly as ozone/smog precursors and directly as environmentally toxic substances with effects that can lead to air pollution such as photochemical smog, ground-level ozone, sick building syndrome, and multiple chemical sensitivities.[3] In enclosed spaces, low concentrations of VOCs can cause shortness of breath, tightness in the chest, loss of appetite and memory, irritation of the eyes, nose and throat, and high concentrations can lead to loss of consciousness, dizziness, and an increased risk of acute poisoning and even death.[4]

Treatment technologies for VOCs are generally based on the recovery or destruction of VOCs.[4] Recovery-based technologies mainly include absorption,

View Article Online
DOI: 10.1039/D5NR01880C

adsorption, condensation and membrane separation. Destruction technologies include direct combustion, biodegradation, catalytic combustion and plasma catalysis. Of these, catalytic combustion consistently offers low cost and high removal rates, positioning it as an efficient, environmentally friendly and cost-effective method for VOCs. Catalytic combustion oxidizes VOCs into CO_2, H_2O and other relatively less harmful compounds. The principle is to reduce the temperature of the direct combustion process through the use of suitable catalysts, which completely destroy the VOCs, and the low temperatures also result in the formation of fewer hazardous products, making it a more efficient and environmentally friendly process than others.

The main challenge in the removal of VOCs by catalytic combustion is the preparation of catalysts with high efficiency, low cost, and low energy consumption. Catalysts used for catalytic combustion of VOCs can be classified into three categories: (1) noble metal catalysts; (2) transition metal oxide catalysts; (3) composite metal oxide catalysts.[4] However, these catalysts need further improvement in terms of catalytic activity and enhanced stability.[5-8] Among the non-precious metal catalysts, perovskite catalysts have attracted attention for exhibiting high activity, high stability, and easily adjustable redox properties, and are one of the most promising catalytic materials in catalytic combustion studies of VOCs. Over the past 25 years, international efforts have been devoted to studying the various applications of perovskite in the catalytic combustion of VOCs (Fig. 1a-b). The structural type of typical perovskite is dominated by ABO_3, and the ideal crystal formation is considered to be a highly symmetric cubic Bravais lattice in the space group Pm-3m. In most cases, however, this ideal condition

View Article Online
DOI: 10.1039/D5NR01880C

may not hold because the structure does not have cubic symmetry, but deforms according to the ionic radii, interatomic distances, and stacking of the elements A, B, and O to form crystal structures such as orthorhombic, rhombohedral, monoclinic, and rhombohedral phases (Fig. 2a-f). Such distortions are quantified by the tolerance factor $t=(r_A+r_O)/\sqrt{2}(r_B+r_O)$, where r_A, r_B, and r_O denote the ionic radii. When the value of t is between 0.8 and 1.0, the perovskite structure can exist stably; when t is close to 1, the crystal structure approaches the ideal cubic crystal system; when the value of t is greater than 1, the crystal structure will be distorted and non-cubic crystal system structures.[9] The A-site is typically occupied by rare-earth or alkaline-earth metal elements with large ionic radii that adopt twelve-coordinated oxygen configurations (e.g., Ca, Sc, Sr, La, Ce), while the B-site is predominantly filled by transition metal elements possessing smaller ionic radii in six-coordinated oxygen environments (e.g., Ti, Mn, Fe, Co, Ni).[9] A and O form a cubic stack and B is contained in an octahedral void in the stack. The ABO sites can be doped simultaneously, the A and B sites can be doped with other metal ions of similar radii, and the O site can be doped with elements such as N, F, Cl and S.[10] The cation in the A-site acts to stabilize the crystal structure. The transition metal ions at the B-site are the main factors affecting the structural properties, redox properties, and stability of perovskite oxides, while the A-site ions are not directly involved in the catalytic reaction, and change the overall catalytic performance of perovskite by influencing the electronic structure, defect structure, and surface properties of the B-site cations. The unique crystal structure, electronic structure and other properties of perovskites make them very promising as alternative catalysts.

View Article Online
DOI: 10.1039/D5NR01880C

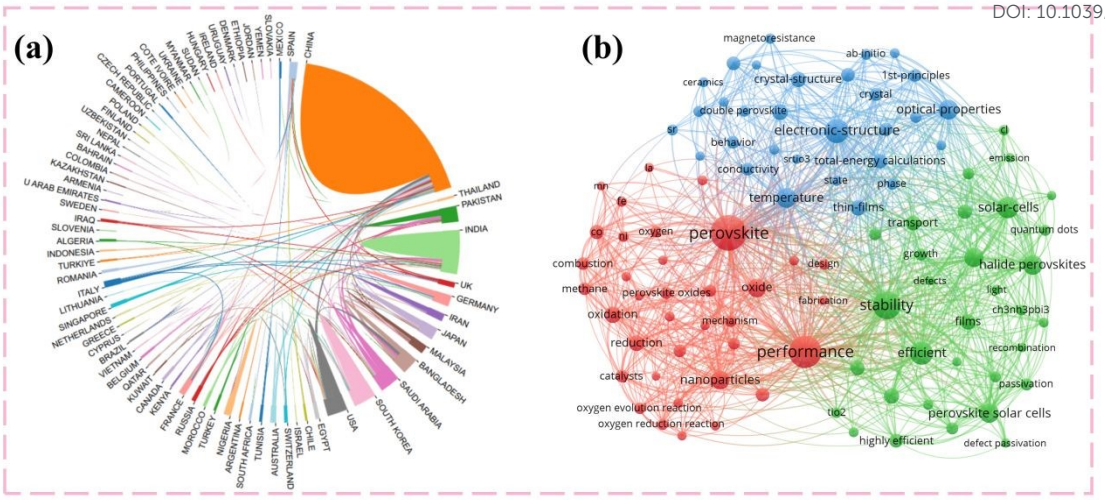

Fig. 1. (a) International Exploration and Cooperation on Perovskites and VOCs from 2000 (1 January) to 2024 (31 December). **(b)** Literature on perovskite, catalytic combustion of VOCs and electronic structure of perovskites published between 2005 (1 January) and 2025 (31 March). Co-occurrence diagram.

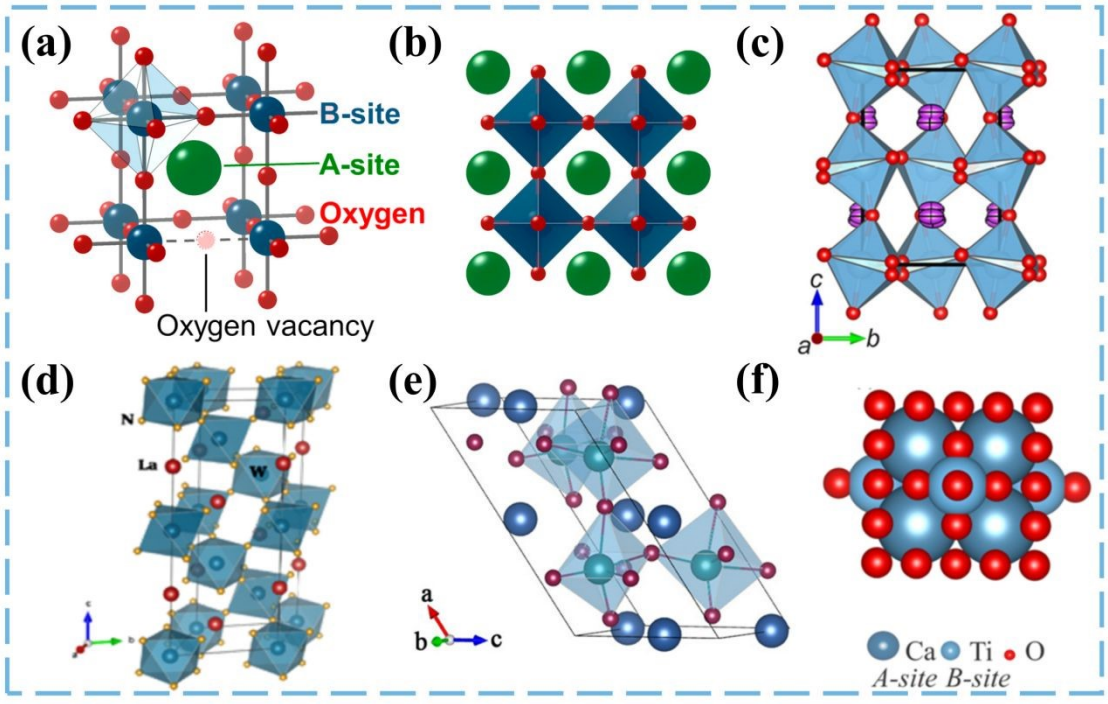

Fig. 2. (a) Illustration of a unit cell of the perovskite structure. **(b)** A cubic perovskite.[11] **(c)** An orthorhombic perovskite.[12] **(d)** A rhombohedral perovskite.[13] **(e)** A monoclinic

View Article Online
DOI: 10.1039/D5NR01880C

phase perovskite.[14] **(f)** A rhombohedral-phase perovskite.[15]

Although previous reviews on the catalytic combustion of VOCs have focused on perovskite catalysts, there is still a significant gap in systematic reviews addressing the modulation of the electronic structure of perovskites. In this paper, by integrating the research progress in recent years, the regulatory mechanism of perovskite catalysts on the catalytic combustion performance of VOCs is revealed for the first time from the perspective of perovskite electronic structure. We establish conformational relationships between four electronic dimensions and macroscopic catalytic behavior:(1) cation defects optimize the B-O electronic structure by modulating e_g-orbital occupancy, d/p-band center displacement and oxygen vacancy generation; (2) Modulation of the adsorption/activation process of VOCs by the effect of hybridization of the elemental d-orbitals at the B-site with the p-orbitals at the O-site; (3) Oxygen vacancies enhance reactant adsorption/activation by affecting orbital filling and oxygen 2p orbital center near the Fermi energy level; (4) A systematic summary of the microscopic mechanisms by which other components of VOCs (H_2O, Cl, S) affect catalytic stability and activity through toxication. By systematically resolving the enhancement mechanisms of doping modification (elemental substitution at A/B/O sites), surface reconstruction (acid-base etching) and other strategies, the relationship between electronic structure parameters (d-band center positions, oxygen vacancy concentrations, charge transfer barriers, etc.) and catalytic performance was elucidated. Looking ahead, the integration of machine learning-based high-throughput electronic structure design and dynamic characterization techniques under operating conditions

View Article Online
DOI: 10.1039/D5NR01880C

will drive the development of a new generation of perovskite catalysts for research.

2. Mechanisms of catalytic combustion of VOCs

At sufficiently high reaction temperatures, catalytic oxidation produces mainly CO_2 and H_2O according to the following reactions:

$$C_xH_y + (x + \frac{y}{4})\, O_2 \rightarrow x\, CO_2 + \frac{y}{2}\, H_2O \quad (4)$$

Currently, there are three main categories of mechanisms for the complete catalytic oxidation of VOCs: (i) Mars-van Krevelen (MvK), (ii) Langmuir-Hinshelwood (L-H), and (iii) Eley-Rideal (E-R) (Fig. 3).

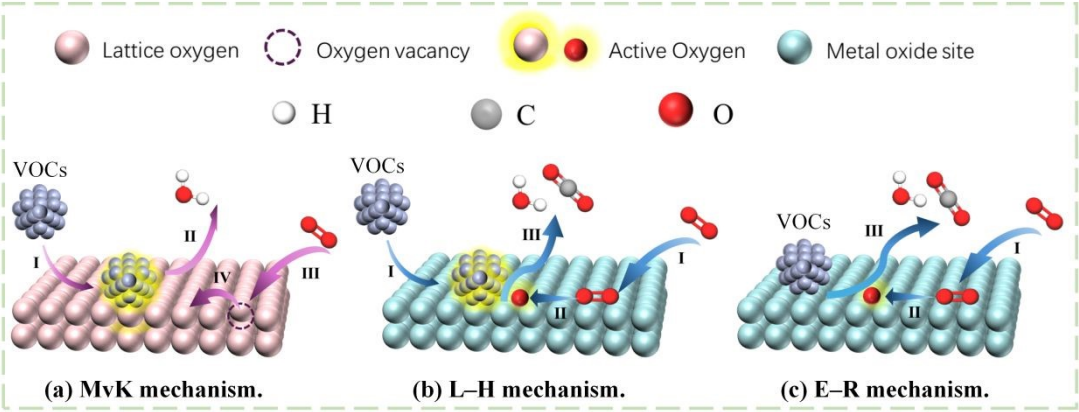

Fig. 3. Schematic diagrams of degradation mechanisms for VOCs oxidation: **(a)** MvK mechanism. **(b)** L–H mechanism. **(c)** E–R mechanism.

For the MvK mechanism, VOCs are first adsorbed on the active sites of the catalyst and react with the surface lattice oxygen of the catalyst to form intermediates, which are eventually converted to CO_2 and H_2O.[16-18] In this process, surface lattice oxygen is reduced and oxygen vacancies are then formed on the catalyst. Subsequently, gaseous oxygen in the feed gas is adsorbed and activated by oxygen vacancies to replenish the depleted surface lattice oxygen. This process results in the catalyst being re-oxidized.

View Article Online
DOI: 10.1039/D5NR01880C

Since the catalyst is first reduced and then re-oxidized, this mechanism is also known as a redox mechanism.

In the L-H mechanism, it is assumed that the reaction occurs between adsorbed VOC and adsorbed oxygen.[19,20] VOCs are also first adsorbed onto the active sites, while gaseous oxygen is activated to reactive oxygen (chemisorbed oxygen) in the presence of the active sites. Subsequently, the VOC molecules are converted to CO_2 and H_2O under the attack of dissociative oxygen and sometimes accompanied by the production of new VOCs.

For the E-R mechanism, the reaction occurs between adsorbed oxygen and reactant molecules in the gas phase.[21,22] The O_2 molecules are adsorbed on the catalyst surface and become "adsorbed molecules", but the VOCs molecules remain in the gas phase.

Catalysts that follow only the E-R mechanism are rare in the catalytic combustion of VOCs. This mechanism is generally found in the low-temperature region of the catalytic combustion reaction.[23,24]

Catalytic combustion reactions of VOCs are complex. In many cases, due to the composition of the feed gas, the nature of the catalyst, the reaction conditions and other factors, VOC molecules tend to react simultaneously with various oxygen species for multiple conversions. Therefore, catalytic combustion of VOCs generally follows a coupled mechanism.[25-27]

View Article Online
DOI: 10.1039/D5NR01880C

3. The influence of perovskite electronic structure on VOC catalytic mechanisms

Perovskite oxides have several outstanding features such as abundant defects, tunable metal-oxygen bond lengths and strengths, high redox capacity of B-site cations, and excellent structural flexibility. These properties are influenced by the electronic structure of perovskite and other components in the VOCs, which alter the activity of the perovskite catalyst.

3.1 Cationic defects

The perovskite lattice can have some degree of cationic defects. The perovskite structure is affected by electroneutrality. The sum of the cation charges should equal the oxygen charge. When partial/total ion substitution fails to achieve this parameter, the different oxidation states lead to defects in the matrix, which may be cationic defects. Typically, perovskites exhibit A-site vacancies. This is because BO_3 forms a stable network in the perovskite structure, and the A-site cations of the 12 coordination sites can be partially deleted.[9] Fig. 4a-c shows some cation-deficient perovskites.[15,31,32] A-site cation deficiency significantly impacts the local arrangement and coordination number of perovskite cations, lattice structure and surface properties, thus affecting the performance of perovskite oxides in various reactions. The A-site defect allows unpaired electrons to occupy empty e_g orbitals and optimizes the overlap state of hybridization between the B-site d orbitals and the 2p orbitals of O, constituting a more efficient electron transfer process. The electronic structure of the B-O bond is optimized to favor the direction of the oxygen redox process, increasing the occupation of the antibonding electrons B-O bond and enhancing the B-O covalency, thus enhancing the

View Article Online
DOI: 10.1039/D5NR01880C

catalytic properties of perovskite.[28,29] E_g orbital occupation can produce spin holes in oxygen through exchange interactions.[30] As a result, the e_g electrons will become delocalized and generate spin channels connecting the B-site cations and O anions, further generating homogeneous spin paths to accelerate charge transfer and thus accelerate VOCs redox reactions.

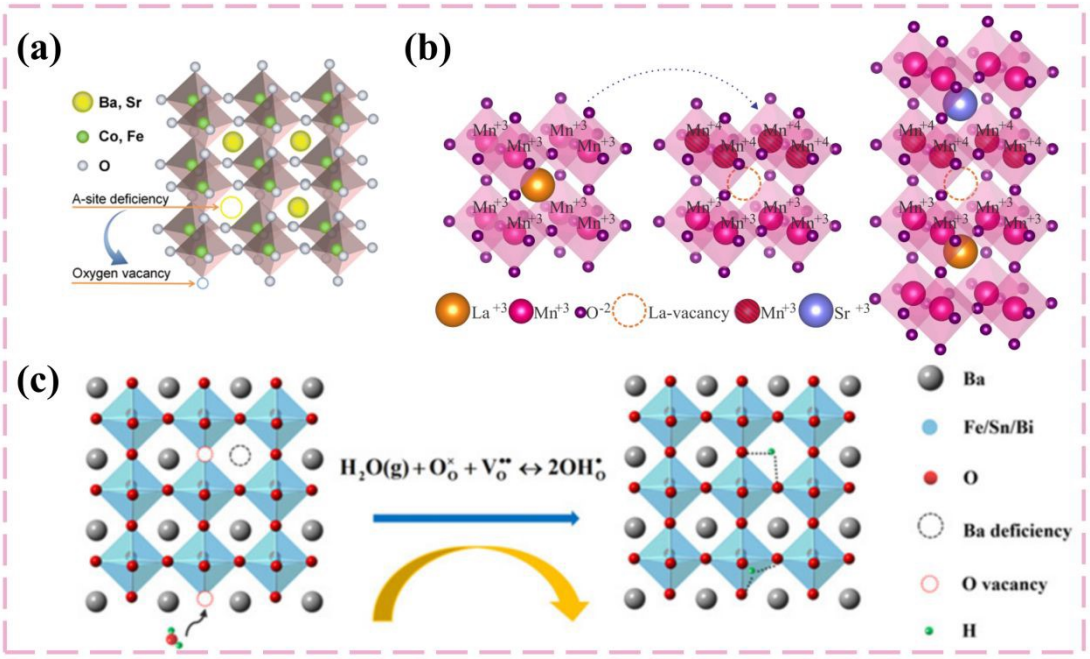

Fig. 4. Some cation-deficient perovskites **(a)** A-site deficient cobalt-based perovskite oxides.[31] **(b)** Schematic of a cationic vacancy formation in a $La_{1-x}Mn_xO_3$.[15] **(c)** A-site deficient cobalt-free barium ferrite-based perovskite.[32]

Furthermore, in the presence of A-site defects, the d-band center moves towards the Fermi energy level (EF) due to the increase in the antibonding state. High-energy antibonding electrons are generally considered to be unstable, leading to e_g-orbital electrons being more active for redox reactions.[33] The p-band center of O-2p also shifts towards the EF energy level, making lattice oxygen more conducive to participating in

View Article Online
DOI: 10.1039/D5NR01880C

the MvK mechanism of VOCs catalytic oxidation. The displacement of A-d and O-2p orbitals suggests that charge transfer between B and O-related adsorbates (O^{2-} and O_2^{2-}) is accelerated in A-site-deficient perovskites, promoting the oxidation of B species.[34,35] A cationic defect at position A causes the d band center to shift towards the Fermi level (EF), rendering high-energy antibonding electrons unstable. This leads to greater reactivity of the e_g orbital electrons in redox reactions, increases the hybridization degree of the B-d and O-2 p orbitals, enhances the bending vibration of oxygen, and facilitates charge transfer from position B to position O. This activates the O_{latt} near the A defect, thereby enhancing the catalytic oxidation activity for VOCs.[36,37] The feasibility of regulating surface reactivity by adjusting A-site cation vacancies can modify the electronic structure characteristics of lanthanum manganite perovskites (Fig. 5a-d). [38] The introduction of La defects into $LaMnO_3$ will result in the partial reduction of Mn^{4+} to Mn^{3+} and the unpaired electrons will fill the empty e_g orbitals. Occupation of e_g orbitals can produce spin holes in oxygen through exchange interactions. As a result, the e_g electrons will leave the domain and generate spin channels connecting the Mn cations and O anions, further generating uniform spin paths to accelerate charge transfer and thus redox reactions. In the presence of La defects, the d-band center moves towards the Fermi energy level (EF) due to the increase in the antibonding state. High-energy antibonding electrons are unstable, which leads to e_g orbital electrons being more active for redox reactions. The displacement of Mn-3d and O-2p suggests that charge transfer between Mn- and O-related adsorbates (O^{2-} and O_2^{2-}) would be accelerated in La-deficient perovskites, facilitating the oxidation of Mn species (Fig.

View Article Online
DOI: 10.1039/D5NR01880C

5e-f). Perovskite $LaMnO_{3.15}$ was prepared by the citric acid sol-gel method, revealing the fundamental relationship between La vacancy and surface lattice oxygen (O_{latt}) activation.[39] The effect of La vacancies (V_{La}) on the electronic structure of MnO_6 is twofold: (1) the increase in Mn valence leads to further simplification of the e_g orbitals and a decrease in the orbital ordering of the e_g electrons, thus weakening the J-T distortion of $LaMnO_{3.15}$. (2) Mn-O shortening, increased hybridization of Mn-3d and O-2p orbitals, enhanced bending vibrations of oxygen, and enhanced octahedral distortion. The result is that Mn in the MnO_6 octahedron transfers charge to O more readily, thereby activating O_{latt} near V_{La} (Fig. 5g-h). In general, shorter Mn/O bond length shortening implies shorter interatomic distances and rapid interfacial transfer of charge to the reaction sites, which promotes the redox properties of perovskite $LaMnO_{3.15}$.

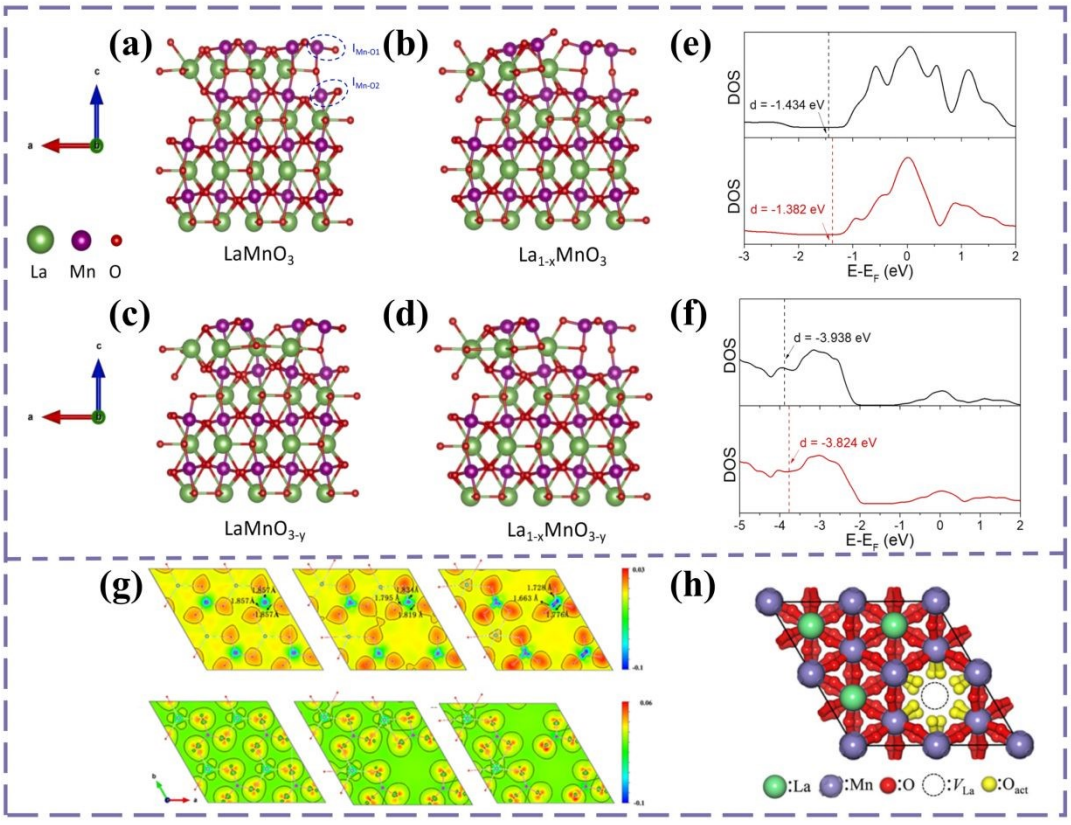

View Article Online
DOI: 10.1039/D5NR01880C

Fig. 5. (a) $LaMnO_3$. **(b)** $La_{1-x}MnO_3$. **(c)** $LaMnO_{3-y}$. **(d)** $La_{1-x}MnO_{3-y}$. **(e)** d-band centers of Mn on $LaMnO_3$ and $La_{1-x}MnO_3$ perovskite. **(f)** p-band centers of O on $LaMnO_3$ and $La_{1-x}MnO_3$ perovskite.[35] **(g)** Difference in charge density of Mn atoms and O atoms. **(h)** Model of La vacancies induced activation of surface lattice oxygen.[39]

B-site cation defects may be caused by vacancies, substitutions or interstitial exchanges of cations in the crystal structure.[40] Although there are some examples showing B-site defects, this type of defect in perovskite oxides is uncommon, which may be related to the fact that defects in the B-site cations of perovskite oxides are less energetically favorable. Indeed, the activity of perovskite oxides can sometimes be further improved by introducing a small number of B-site cation defects into the oxide lattice, and this improvement can enhance oxygen mobility and thus surface exchange and overall diffusion.[41]

3.2 Electronic structure of elements at the B-site

The B-site transition metal element is usually considered to be the main factor influencing the activity of perovskite oxides. The Sabatier principle postulates that an optimal catalyst must exhibit moderate adsorption strength with reactants--neither too weak to limit activation nor too strong to hinder desorption. If the bonds are too weak, the catalyst and the reactants hardly interact with each other, whereas if the bonds are too strong, the reactants do not desorb from the catalyst surface, thus effectively inhibiting further reactions. Using molecular orbital theory, the ORR (oxygen reduction) activity of perovskite catalysts is mainly related to the degree of σ*-orbital (e_g) occupancy and covalency of transition metal oxygen at the B-site.[28] Their experiments

View Article Online
DOI: 10.1039/D5NR01880C

showed that e_g-filling and metal-oxygen covalency have a key influence on the competition between O_2^{2-}/OH^- substitution and OH^- regeneration on surface transition metal ions as the rate-limiting step of ORR. Perovskites with an e_g orbital occupancy close to 1 contribute significantly to the covalent B-O_2^{2-} bond and achieve stable adsorption through exchange, resulting in faster VOCs oxidation and the highest ORR activity. Too few σ* orbitals occupied ($e_g < 1$) or too many occupied ($e_g > 1$) result in interactions with adsorbed oxygen that are either too strong or too weak. As mentioned in Section 2, this inhibits the catalytic oxidation of VOCs, resulting in lower ORR activity. In addition to e_g filling and metal-oxygen covalency, other electronic structure factors of the B-site transition metals, such as the number of d electrons, the position of the d-band center, and the oxidation state also affect perovskite reactive activity. The interaction of the external B-site orbitals (s and p) and the anionic 2p orbital produces valence and high energy bands because the internal d orbitals of the B-site are held at the bandgap energy, which is the energy necessary for the electron to reach the conduction band.[15] Since the d orbitals of transition metal ions in the B site have multiple energy levels, the band structure of perovskites is relatively complex, with multiple bands and band gaps. The size and distribution of these band gaps determine the catalyst's ability to adsorb VOCs and the recombination rate of electron-hole pairs. Thus, the electron transport properties are realized due to the d orbital of the B site. The excellent redox properties of perovskite oxides are mainly related to the abundant valence of the B-site transition metal ions, which upon substitution produce changes in lattice vacancies and/or valence states of the B-site ions, thus providing flexible and

View Article Online
DOI: 10.1039/D5NR01880C

tunable electronic structures for the perovskite oxides.[42]

3.3 Oxygen Vacancy

According to the principle of electroneutrality, desorption of lattice oxygen leads to an increase in the oxidation state of the B-site cation (assuming that the valence of the A-site cation is unchanged), and thus it is closely related to the redox capacity of the B-site cation. Desorption of lattice oxygen usually occurs at temperatures higher than 700 °C because of the high bond energy of the B-O bond, which is the source of oxygen vacancies in the structure.[43] In the catalytic oxidation reaction of VOCs, oxygen vacancies are one of the key factors, providing a place for oxygen adsorption and activation. Adsorption of oxygen from the gas phase and further doping of oxygen atoms within the lattice typically results in three types of charged oxygen, namely, O^{2-}, O^{-}, and O^{2-}. These reactive oxygen species react with VOCs, equivalent to lattice oxygen participating in the oxidation of VOCs, causing the catalyst to be reduced. Subsequently, oxygen in the gas phase can replenish oxygen vacancies, restoring the catalyst to its initial state, completing the catalytic cycle and achieving efficient oxidation of VOCs. This is highly consistent with the MvK mechanism. The introduction of such lattice defects leads to several changes in the chemical and transport properties of perovskite, which directly or indirectly alter the catalytic properties. Orbital filling and the position of oxygen 2p orbital centers near the Fermi level elucidate how oxygen vacancies enhance reactant adsorption/activation, electrical conductivity and lattice oxygen mobility.[44,45] Both the top edge of the O-2p band and the Fermi energy level are lowered when oxygen vacancies are present, another

View Article Online
DOI: 10.1039/D5NR01880C

indication of an electron donor. On the other hand, oxygen vacancies can reduce the energy gap between the metal d-band and the p-band center of O, thus increasing the covalent metal-oxygen bonding.[46] The more covalent systems there are the greater the concentration of vacancies. Oxygen-deficient perovskite $SrFeO_{3-\delta}$ ($0.02<\delta<0.26$) was synthesized for methane combustion, with comprehensive characterization employing X-ray/neutron powder diffraction, thermal analysis under reducing conditions, temperature-programmed reduction/desorption (TPR/TPD), BET surface area measurements, and X-ray photoelectron spectroscopy (XPS).[47] The results show that in the absence of mass transfer phenomena, the rate of reaction was found to be strongly correlated with the number of oxygen vacancies present in the perovskite structure: The highest activity was found in the highly defective $SrFeO_{2.74}$ sample, which accommodated the highest proportion of O vacancies (Fig. 6a-b). Oxygen vacancies in perovskite oxides can be introduced by cationic or anionic doping or defects. $La_{1-x}Sr_xNiO_3$ was prepared and tested it in methane combustion.[48] The results demonstrate that partial substitution of Sr by La alters the oxide stoichiometry, generating a mixture of Ni^{I}/Ni^{III} oxidation states and oxygen vacancies along with surface enrichment of Sr-containing phases, revealing that the surface composition and oxygen nonstoichiometry predominantly govern the catalytic activity in the target reaction (Fig. 6c-d). Anion doping has a direct effect on the oxygen vacancy concentration. When ions directly displace lattice oxygens, they maintain electroneutrality in the system by lowering the oxidation state of neighboring metal cations and losing lattice oxygens, which leads to an increase in the oxygen vacancy concentration. Rapid oxygen exchange at the

View Article Online
DOI: 10.1039/D5NR01880C

reaction interface can rapidly improve the properties of perovskite materials, which is advantageous for driving catalytic reaction kinetics.[49] Anionic doping can also further enhance the flexibility of its components, thus potentially improving the performance of catalytic oxidation reactions.[50]

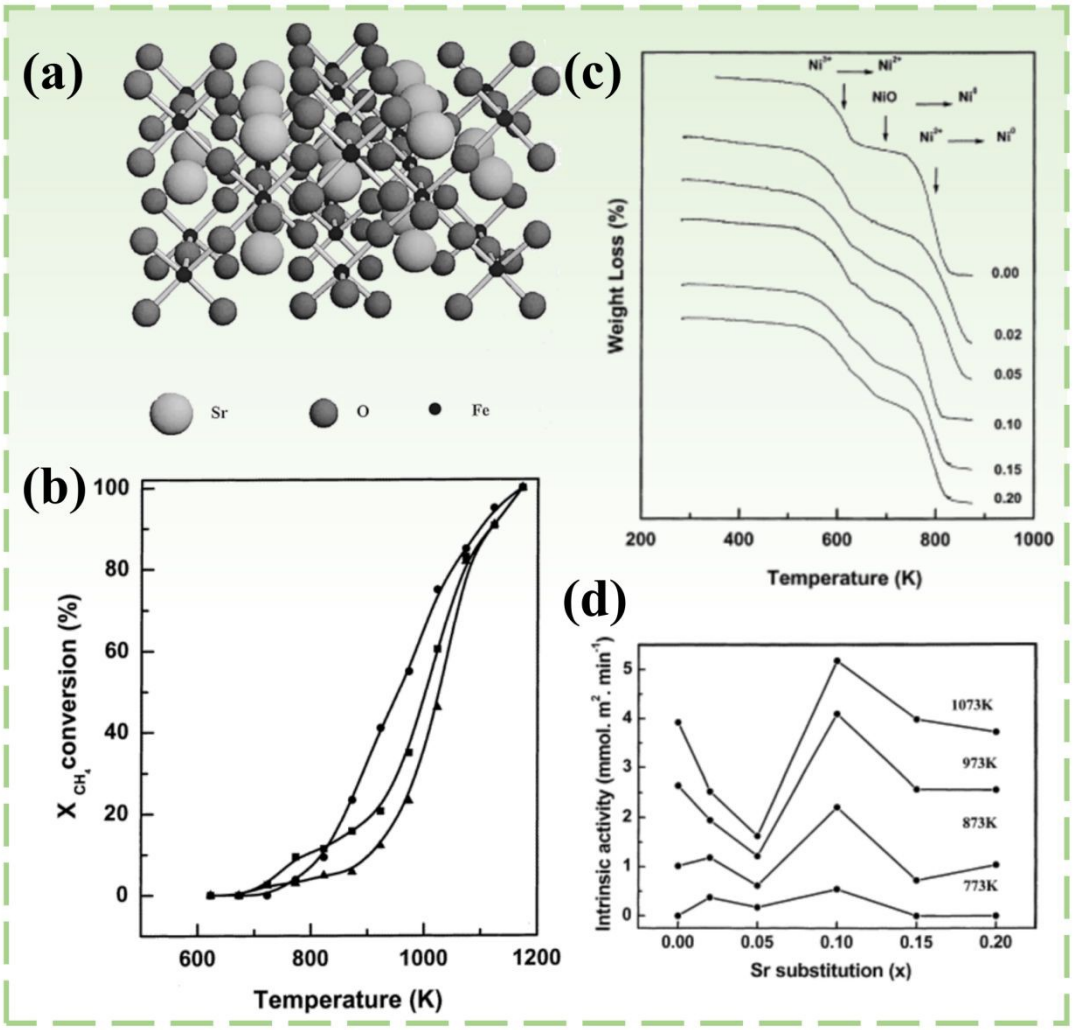

Fig. 6. (a) View of the crystal structure of $SrFeO_{2.74}$. **(b)** Temperature dependence of CH_4 conversion on $SrFeO_{3-\delta}$: (·) δ = 0.26, (▪) δ = 0.09, and (▲) δ = 0.02 oxides.[47] **(c)** the reduction thermograms of all the catalysts. **(d)** Influence of the substitution degree (x) on the intrinsic activity of calcined $La_{1-x}Sr_xNiO_3$ catalysts (x=0.10, the oxygen non-stoichiometry value (δ) reached a maximum).[48]

View Article Online
DOI: 10.1039/D5NR01880C

3.4 Impacts of other components of VOCs

3.4.1 The effect of water on the electronic structure of perovskite

Water vapor is an important component of industrial exhaust gases and catalyst activity is often affected by water vapor. The effect of water on the catalyst is complex, as water or hydroxyl groups accumulate in the active sites of the catalyst, competing with the VOCs for adsorption and hindering the catalytic oxidation process, but water is also sometimes used as a detergent for the removal of by-products from the surface of the catalyst, or it can be used to oxidize the VOCs through certain reactions, which can have a facilitating effect on the catalytic reaction.[51-54] Fig. 7a-b shows schematic illustration of the interaction between water molecules and perovskites. Under low humidity conditions, a small number of water molecules interact with organic cations (MA^+) on the surface mainly through hydrogen bonding, forming a weak physisorption. After adsorption on the perovskite surface, water molecules dissociate into H^+ and OH^-, where OH^- preferentially occupies the surface oxygen vacancies. The formation of hydroxyl groups (-OH) reduces the concentration of surface oxygen vacancies and inhibits the mobility of lattice oxygen. The electron-donating inducing effect of the hydroxyl group can locally change the electron cloud density of the B-site metal, weakening the covalency of the B-O bond through the inducing effect, leading to an increase in the number of e_g-orbital electrons occupied by the B-site ions, and decreasing their oxidative capacity. However, when the ambient humidity increases and the number of water molecules increases, the water molecules will not only cover the entire surface of the perovskite but also gradually penetrate into the interior of the

View Article Online
DOI: 10.1039/D5NR01880C

perovskite. Theoretical calculations show that water molecules have a low diffusion energy barrier inside perovskite and can enter the interior of perovskite with relative ease. H_2O penetrates into the perovskite lattice interstitials, triggering local lattice expansion. This distortion alters the B-O-B bond angle and weakens the efficiency of electron transfer to adsorbed oxygen by modulating the degree of d-p orbital hybridization and shifting the conduction band bottom (CBM) upwards.[53,55,56] Study has shown that H_2O reacts with chemisorbed oxygen to form hydroxyl groups, which occupy the available active sites for toluene adsorption and compete with toluene molecules for adsorption, while at the same time H_2O depletes the chemisorbed oxygen from the catalyst, thus inhibiting toluene oxidation (Fig. 7c).[57] In addition, the effect of water on the catalytic toluene combustion by La-Sr-Co-Fe-O perovskite-type oxides was investigated.[18] The results showed that toluene conversion decreased slightly to 95% and 86% at 300℃ with the introduction of 5 vol% and 10 vol% H_2O in the reaction gas, respectively. When H_2O was removed, the toluene conversion returned to its initial value, indicating that the decrease in catalytic performance was reversible (Fig. 7d). The introduction of H_2O may hinder the formation of structural water on the perovskite surface, which reduces the number of oxygen vacancies, decreases oxygen mobility, and ultimately reduces the catalytic performance.

View Article Online
DOI: 10.1039/D5NR01880C

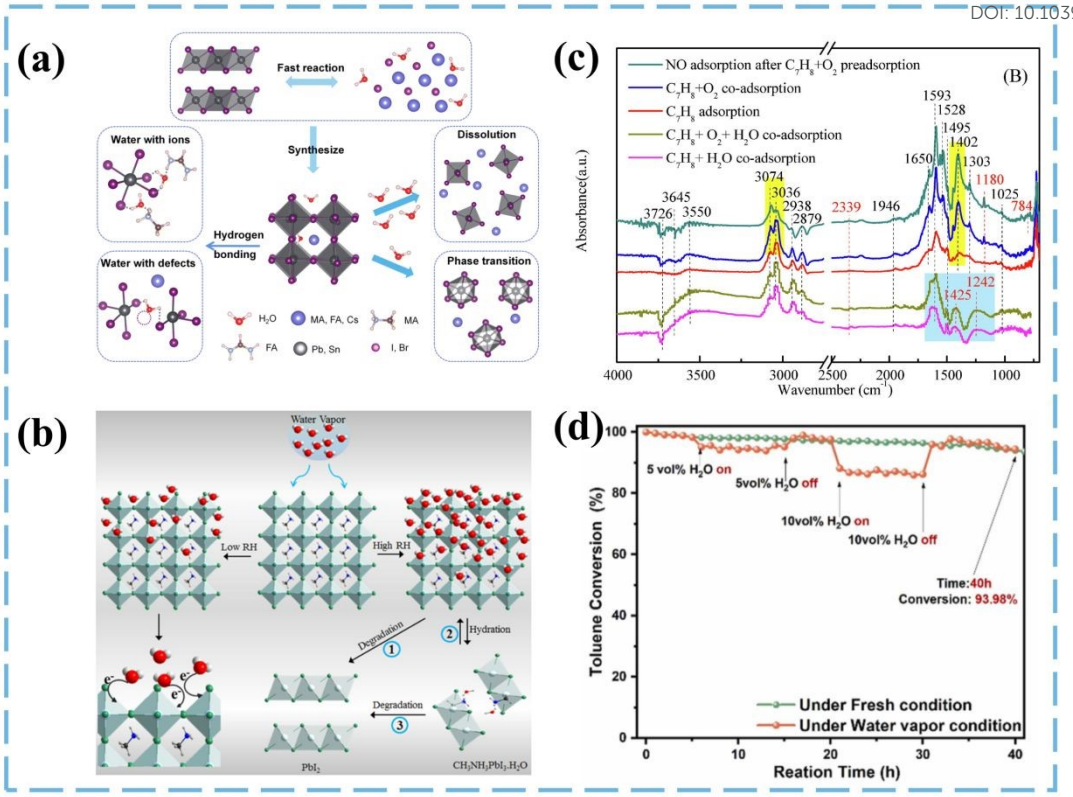

Fig. 7. (a-b) Illustration of the perovskite–moisture interaction.[56,58] **(c)** The in situ DRIFTS study on the reaction mechanism of simultaneous oxidation of toluene over the $La_{0.65}Co_{0.35}FeO_3$ perovskite in the absence and presence of H_2O.[57] **(d)** the effect of H_2O on the catalytic activity of LSCF was investigated at 300 °C.[18]

In the catalytic combustion of chlorinated volatile organic compounds (Cl-VOCs), deposited Cl species tend to bind to H_2O, facilitating the migration of dissociated Cl species and inhibiting the formation of chlorination by-products. Water decomposition also provides abundant H atoms for dechlorination and hydroxyl groups for deep oxidation of intermediates.[59] The deposition of polychlorinated by-products on the catalyst surface was also significantly reduced under humid conditions, suggesting a washing effect of water.[60]

View Article Online
DOI: 10.1039/D5NR01880C

3.4.2 The effect of chlorine on the electronic structure of perovskites

Cl-VOCs have more severe toxicity, high chemical stability, and low biodegradability, and their accumulation in various environmental factors can lead to water, soil, and air contamination, and ultimately to transfer to living organisms. Cl migration pathways during catalytic oxidation include HCl desorption assisted by the Brønsted acidic center, Cl_2 formation via the Deacon reaction, chlorination to produce organic by-products and deposition on the catalyst surface.[59] Perovskite has attracted the attention of researchers due to its excellent structural stability, but in practice, perovskite catalysts used for the catalytic combustion of Cl-VOCs are prone to deactivation due to chlorine deposition caused by polychlorinated by-products clogging the active sites.[61-63] Weak hybridization of the 3p orbitals of Cl with the metal d-orbitals leads to reduced electron delocalization in the metal-oxygen network. The electron-withdrawing effect of chlorine withdraws electrons from the B-site metal through metal-Cl bonds, resulting in elevated oxidation states of metal centers, hindered charge transfer dynamics, and ultimately diminished redox capacity.[64] In addition, although Cl causes a decrease in the oxygen vacancy formation energy, the large size of Cl^- can block the oxygen vacancies, which manifests itself in a deterioration of the catalytic activity despite the lattice distortion and the decrease in the oxygen vacancy formation energy.[65,66]

The problem of catalyst deactivation due to Cl poisoning, excluding pore clogging and active site occupation caused by chlorine species, metal chlorination is the key causative factor for Cl poisoning. Metal chlorination reduces active sites and surface

View Article Online
DOI: 10.1039/D5NR01880C

oxygen, the interaction of Cl species with the metal surface leads to volatilization of the active phase metal, and the formation of HCl and Cl_2 leads to rusting of the catalytically active metal.[59] It has been shown that the synergistic effect of acidity and redox capacity is an important support for the catalyst to have a strong degradation ability.[67] Surface oxygen and oxygen mobility are key to the redox capacity of the catalyst. In addition, maintaining sufficient active sites is important for the catalytic oxidation of Cl-VOCs.

3.4.3 The effect of sulfur on the electronic structure of perovskite

Exhaust gases from VOCs emitted in specific industrial environments (pharmaceutical factories, petrochemical industry and wastewater discharge plants) usually have sulfur-containing substances, and even after desulphurization, a small amount of sulfur will still be present. During the oxidation reaction, sulfur-containing substances may occupy the active sites on the catalyst surface, leading to temporary physical deactivation of the catalyst. If these substances adsorb onto the perovskite surface and react with the active sites, they can lead to catalyst poisoning and permanent failure.[68] It has been shown that SO_2 molecules prefer to adsorb on a single ligand oxygen O in the form of an S-O double bond, taking into account the stability of the adsorption structure and the electronegativity of each element. Mulliken population analyses show that S is oxidized not only by the O atoms on the surface but also by the O atoms of SO_2, reacting to form sulphate, sulfite or sulfide. The s-state of adsorbed SO_2 broadens and moves away from the Fermi energy level compared to free SO_2. By comparing the distribution of the p-state of O at the top of the valence band, it is clear

View Article Online
DOI: 10.1039/D5NR01880C

that the position of the p-state is lower and further away from the Fermi energy level after the adsorption of SO_2 than before the adsorption of SO_2. The position of the top of the valence band away from the Fermi energy level indicates lower reactivity. These results confirm that the oxidation of the O site is reduced after sulfite formation.[69-72] These unstable substances also deposit on the catalyst surface and cover the active sites, blocking the pores and preventing the adsorption and diffusion of reactive gases, and at higher concentrations may destroy the perovskite crystal lattice and cause irreversible poisoning.[73,74]

4. Methods of modulating the electronic structure of perovskite

Both bulk phase and surface modifications of perovskite can effectively modulate the electronic structure of perovskite and enhance its catalytic activity. Table 1 summarizes the modification methods and catalytic performance of the different perovskite catalysts used for the catalytic combustion of various VOCs mentioned in this section.

Table 1. Modified perovskites employed in the catalytic oxidation of VOCs.

VOC	Catalyst	Space velocity	Modification method	$T_{90\%}$ (°C)	Ref.
Methane	$La_{0.7}Ce_{0.3}FeO_3$	12,000 ml g_{cat}^{-1} h^{-1}	A-site doping	510	75
Vinyl Chloride	$La_{0.8}Ce_{0.2}MnO_3$	15,000 h^{-1}	A-site doping	213	76
Toluene	$LaNi_{0.75}Co_{0.25}O_3$	18,000 h^{-1}	B-site doping	225	77
Vinyl Chloride	$LaNi_{0.2}Mn_{0.8}O_3$	15,000 h^{-1}	B-site doping	210	78
Propane	$LaCo_{0.97}P_{0.03}O_3$	42,857 h^{-1}	B-site doping	376	79
Toluene	$La_{0.8}Ce_{0.2}Mn_{0.8}Ni_{0.2}O_3$	18,000 h^{-1}	A-Site and B-Site Co-Doping	350	80
Toluene	$La_{0.5}Sr_{0.5}Co_{0.8}Fe_{0.2}O_3$	30,000 mL g^{-1} h^{-1}	A-Site and B-Site Co-Doping	270	18
Toluene	LCO-2F	100 mL min^{-1}	O-site doping	238	81
Methane	$LaFeO_3$	200 mL min^{-1}	Nitric acid etching	593	82
Propane	$La_{0.8}Sr_{0.2}CoO_3$	40,000 mL g^{-1} h^{-1}	Diluted oxalic etching	430	83
Toluene	Rod-like $MnO_2/LaMnO_3$	60,000 mL g^{-1} h^{-1}	Alkaline Hydrothermal and Acid-Etching Treatment	236	84

View Article Online
DOI: 10.1039/D5NR01880C

4.1 Bulk phase modifications

4.1.1 A-site doping

In general, the A-site cations are not directly involved in the catalytic reaction and are used to change the overall catalytic properties of perovskite by influencing the electronic structure, defect structure and surface properties of the B-site cations. In perovskite oxides, A-site doping changes the potency of the B-site elements and also increases the number of active sites towards the ORR and the oxygen vacancies on the surface (Fig. 8a).[15,85] Doping A-site ions induces lattice distortion owing to differences in ionic radii. The induced lattice distortion adjusts the intensity of the hybridization of the B-site metal d-orbitals with the 2p orbitals of the O. The mechanism involves B-O bond shortening, reduced orbital ordering, and enhanced octahedral distortion, culminating in an enhancement of the hybridization of the B-3d and O-2p orbitals.[86-89] The shortened B-O bond length implies shorter interatomic distances and rapid interfacial transfer of charge to the reaction site, which promotes the redox properties of perovskite. A-site doping may induce a B-site metal spin state transition. The B-site ions with high spin states have stronger e_g-orbital participation in the reaction, which promotes the adsorption activation of O_2 and thus enhances the oxidation efficiency of VOCs.

Most surface-catalyzed reactions depend to a large extent on the degree of e_g orbital filling. The reduction in e_g occupancy favors the capture of electrophilic absorbers. Guo et al. investigated the structural and property changes of perovskite doped with Sr at the A-site.[90] The d-p hybridization of Co-3d and O-2 p induces a Co

View Article Online
DOI: 10.1039/D5NR01880C

1 s → 3d quadrupole jump (Fig. 8b). For $LaCoO_3$, the 1 s → 3d jump splits into two distinct bands, 1 s → e_g (high energy) and 1 s → t_{2g} (low energy) (Fig. 8c). However, Sr doping causes the pre-edge adsorption of the sample to be an overlap of e_g and t_{2g}, showing a single broadband instead of two separated broadbands, with reduced e_g filling and extended Co-O distance. Therefore, the partial substitution of Sr^{2+} for La^{3+} leads to an increase in the octahedral symmetry of [CoO_6] as well as favors the improvement of perovskite adsorption properties. The substitution of Sr^{2+} for La^{3+} produces positive holes which are captured by the lattice O^{2-}, resulting in O_2^-/O_2^{2-} species and leaving oxygen vacancies. The positive charge imbalance induced by Sr^{2+} is compensated by a combination of tetravalent Co (IV) ions and oxygen deficiency, which enhances perovskite's reducibility and oxygen mobility.

Partial doping of A-site cations in perovskite oxides promotes the oxidation of VOCs, which has been demonstrated by many researchers. For example, compounds in which the La atom at the A site is partially replaced by a Ce atom.[75] The researchers prepared a series of $La_{1-x}Ce_xFeO_3$ (x=0-0.5) perovskites for the catalytic combustion of methane using a sol-gel method. The results showed that the doping of Ce led to a significant increase in the catalytic activity of $LaFeO_3$. The doping of Ce^{4+} ions increases the number of electrons of Fe ions in $La_{0.875}Ce_{0.125}FeO_3$, which leads to enhanced interactions with $O_{2,ads}$, increased adsorption energy of O_2 on $La_{0.875}Ce_{0.125}FeO_3$, and activation of O-O bonds. Thus Ce-doped perovskite has higher oxidation activity than pure $LaFeO_3$ (Fig. 8d). $LaMnO_3$ and $La_{0.8}A_{0.2}MnO_3$ (A = Sr, Mg, Ce) perovskites synthesized by a co-precipitation method were used for the catalytic

View Article Online
DOI: 10.1039/D5NR01880C

oxidation of vinyl chloride.[76] The doping of Mg and Ce increased the specific surface area of perovskite to adsorb more oxygen on its surface, thus enhancing the catalytic activity of perovskite for vinyl chloride (Fig. 8e). In addition, the doping of Mg and Ce increased the average oxidation state of Mn, increased the crystal defects and produced a higher number of oxygen vacancies, thus improving the redox capacity and oxygen mobility of the Mn^{4+}/Mn^{3+} redox pair. However, Sr doping minimizes the concentration of O_β (oxygen-containing groups, including OH^- or CO_3^{2-} and surface-adsorbed oxygen) in perovskite leading to a decrease in catalytic activity. A-site doping can reduce the inhibition effect of water in the gas on the catalytic oxidation reaction of VOCs and improve the water resistance of the catalyst.

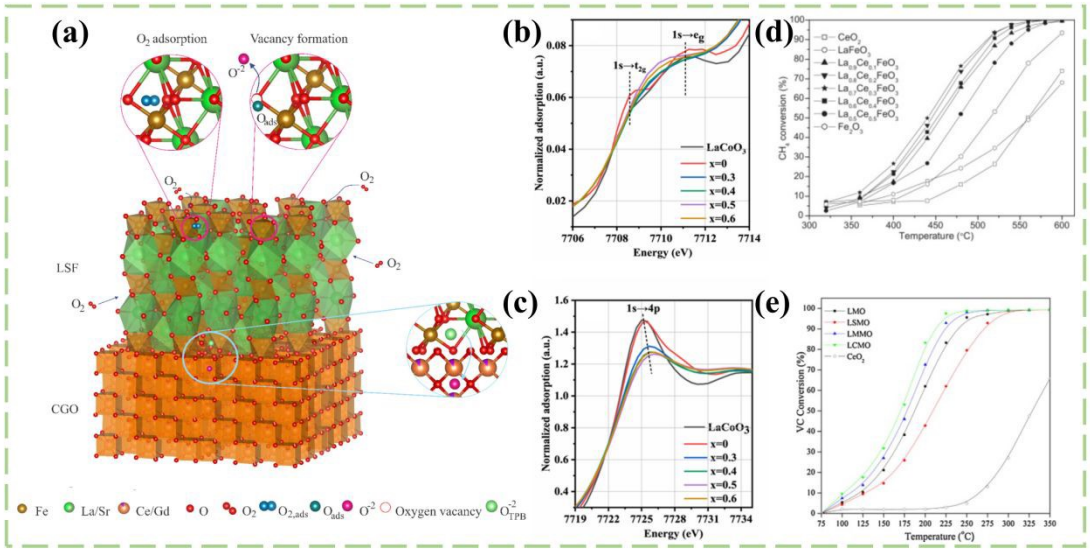

Fig. 8. (a) Sr-doping on $LaFeO_3$, leading to oxygen vacancy formation.[15] **(b-c)** Normalized Co–K edge XANES spectra of the $LaCoO_3$ and $La_{1-x}Sr_xCo_{0.8}Fe_{0.2}O_3$ samples.[90] **(d)** Catalytic activities of $La_{1-x}Ce_xFeO_3$, CeO_2 and Fe_2O_3 samples for methane combustion.[75] **(e)** VC conversion as a function of reaction temperature over $LaMnO_3$ and $La_{0.8}A_{0.2}MnO_3$ (A = Sr, Mg and Ce) catalysts.[76]

View Article Online
DOI: 10.1039/D5NR01880C

4.1.2 B-site doping

The catalytic performance of perovskite catalysts mainly depends on the B-site cations. The B-site in perovskite can be doped with transition metals with various oxidation states, such as Fe, Co, Ni, Cu, Mn and so on. Doping of compatible ionic radii in these transition metals will produce additional oxygen vacancies without morphological deformation and can provide better positions for the entire B-site as well as for the O-2p-band center of the perovskite oxide catalysts.[46] B-site doping leads to an enhanced distortion of the BO_6 octahedron, which enhances the hybridization strength of the metal d orbitals with the oxygen p orbitals, significantly increases the electron density around the Fermi energy level, enhances the covalency of the B-O bond, and the e_g orbital occupancy is closer to the theoretical value of 1 [91], which brings the position of the center of the p-band of O closer to the Fermi energy level, which is conducive to the activation of the oxygen molecule (electron transfer), resulting in a higher catalytic activity.[92] Promote charge transfer so that they have more antibonding orbitals and enhance the binding capacity of the active sites to the reactants, thus affecting the activation and delivery of oxygen species, as well as influencing the adsorption properties of VOCs.[92-95] A series of $La_{0.8}Sr_{0.2}Mn_{1-x}Cu_xO_3$ perovskite-type catalysts were prepared by sol-gel method and evaluated the performance of formaldehyde-catalyzed oxidation The introduction of Cu^{2+} resulted in a charge imbalance, which was compensated for by an increase in the Mn^{4+}/Mn^{3+} ratio of the perovskite.[96] The partial substitution of Mn by Cu cations enhances the oxygen mobility of perovskite, which is attributed to the synergistic interaction between Cu and Mn

View Article Online
DOI: 10.1039/D5NR01880C

atoms on the surface. $La_{0.8}Sr_{0.2}Mn_{0.8}Cu_{0.2}O_3$ catalysts exhibited excellent oxygen mobility, thus facilitating the catalytic oxidation of formaldehyde (Fig. 9a). DFT calculations showed that the absolute value of formaldehyde adsorption energy of surface Cu-O sites was higher than that of Mn-O sites. Thus, the surface Cu and O atoms of perovskite act as active sites for formaldehyde adsorption (Fig. 9b-c). During formaldehyde adsorption, electrons are transferred from formaldehyde to the catalyst surface. The catalyst surface acts as an acceptor to gain electrons. Thus, surface cations with high valence states are favorable for accepting electrons and further adsorbing formaldehyde. The Cu dopant promoted formaldehyde adsorption and facilitated the transfer of more electrons from formaldehyde to the catalyst, favoring formaldehyde activation and subsequent oxidation.

Partial doping of B-site cations in perovskite oxides promotes the oxidation of VOCs, which has been demonstrated by many researchers. A series of $LaNi_xB_{1-x}O_3$ (B = Co, Cu) perovskite catalysts were applied to toluene degradation by sol-gel method.[77] The results show that a small amount of Co doping at the B-site of $LaNiO_3$ can significantly improve its toluene degradation, however, the substitution of Cu for Ni cannot effectively enhance its activity (Fig. 9e), probably because the radius of Cu^{2+} is larger than that of Ni^{2+}, and it is difficult to have a large amount of Cu^{2+} to enter the lattice of $LaNiO_3$. The catalyst exhibited the best activity at a Ni/Co molar ratio of 3:1 in perovskite (Fig. 9d). This is due to the partial doping of the B-site causing an increase in surface defects and active sites, an increase in oxygen vacancies, and an increase in oxygen mobility. Zhang et al. prepared $LaMnO_3$ and $LaB_{0.2}Mn_{0.8}O_3$ (B = Co, Ni, Fe)

View Article Online
DOI: 10.1039/D5NR01880C

perovskite-type oxides for the catalytic oxidation of vinyl chloride using a co-precipitation method.[78] Co-, Ni- and Fe-doped perovskites all exhibited catalytic properties superior to those of $LaMnO_3$ chalcogenides (Fig. 9f). This was attributed to the fact that the substitution of Co, Ni and Fe at the B-site produced more Mn^{4+}, which improved the redox capacity of the Mn^{4+}/Mn^{3+} electric pair, and at the same time produced more oxygen vacancies, which improved the oxygen mobility and increased the oxygen adsorbed on the catalyst surface, thus improving the catalytic performance of perovskite. Overall, the main reason why doping transition metals towards the B-site enhances the catalytic activity of perovskite oxides is to increase their reducibility and oxygen mobility. B-site doping is also important for the development of perovskite catalysts with high catalytic efficiency, good stability and chlorine resistance for elimination.

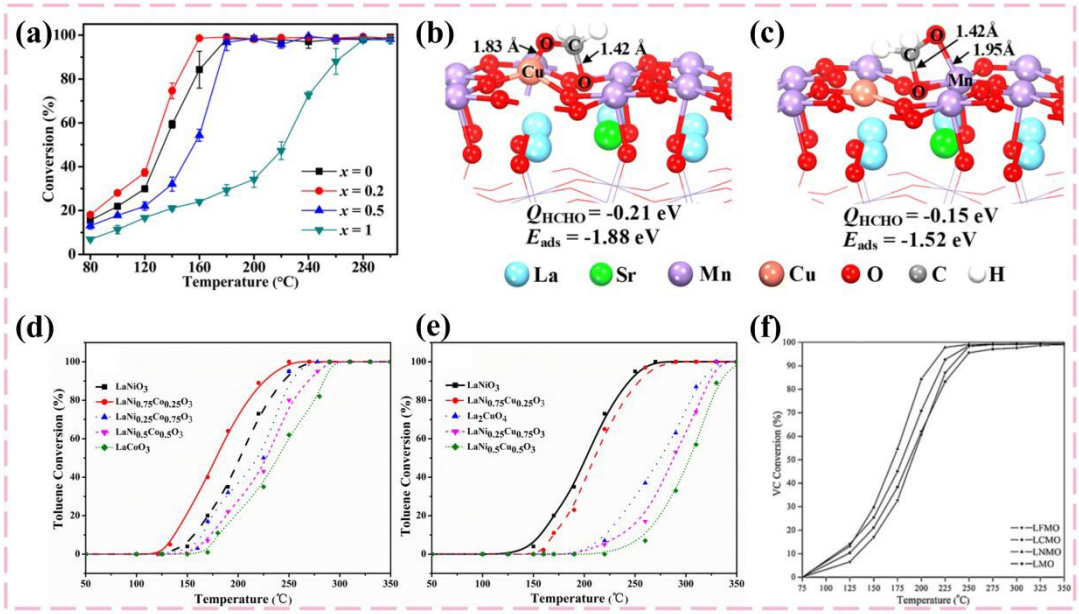

Fig. 9. (a) Catalytic activities of the $La_{0.8}Sr_{0.2}Mn_{1-x}Cu_xO_3$ catalysts. **(b-c)** the optimized configurations and the corresponding adsorption energies (E_{ads}), Mulliken charges (Q),

View Article Online
DOI: 10.1039/D5NR01880C

and structural parameters of formaldehyde adsorption on the surface Cu–O and Mn–O sites.[96] **(d-e)** Catalytic activity of $LaNi_xCo_{1-x}O_3$ and $LaNi_xCu_{1-x}O_3$ perovskite.[77] **(f)** VC conversion as a function of the reaction temperature over $LaMnO_3$ and $LaB_{0.2}Mn_{0.8}O_3$ (B = Co, Ni, Fe) catalysts.[78]

Doping of non-metallic elements (P, S, B and Si, etc.) into the B-site of perovskite oxides can be used to stabilize the perovskite structure. Non-metallic elemental dopants are inherently inert to catalytic reactions. However, non-metallic elemental doping of perovskite oxides usually leads to additional reaction pathways, favorable structural transformations and optimization of the active site.[97] Non-metal (N, P, B, etc.) doping modulates the B-site valence and oxygen vacancies in perovskite. Partial replacement of the B-site metal ion with a highly electronegative nonmetallic element will bring the 3d orbital of B closer to the 2p orbital of O, increasing the metal-oxygen covalent component and thus achieving a lower Fermi energy level. For example, N atoms with low electronegativity and high levels of 2p orbitals can exchange electrons in the 2p orbitals with the 3d orbitals of the B-site active cations. N doping can enhance the oxygen catalytic activity of perovskite $LaCoO_3$.[98] In typical $LaCoO_3$, the Co cation displays a low-spin state with an e_g occupancy of 0. In contrast, in N-LCO, N provides additional electrons to Co via the N-Co bond, resulting in a moderate e_g occupancy of 1 for the Co cation (Fig. 10a). In the case where the O site is replaced by N, the charge distribution around the N-Co bond is more non-local, which favors surface charge transfer (Fig. 10b). The energy difference between the Co-d and O-p band centers decreases from 1.21 eV to 1.17 eV after N doping, indicating that Co 3d-O 2p covalency

View Article Online
DOI: 10.1039/D5NR01880C

has been enhanced (Fig. 10c). It has been demonstrated by many researchers that B-site cation partially doped perovskite oxides with non-metallic elements promote the oxidation of VOCs to some extent. Furthermore, comparing the effects of P-doped and undoped perovskites of $LaCoO_3$ on the catalytic combustion of propane,[79] the results show that doped P modulates the cobalt valence state, leading to a decrease in central symmetry and an enlargement of lattice distortion, which results in the formation of oxygen vacancies and facilitates oxygen migration The electronegativity of P (2.19) is higher than the electronegativity of Co (1.88), which brings the 3d energy band of Co closer to the 2p energy band of O, increases the covalent component, and improves oxygen mobility. The peripheral valence electrons of P can only coordinate with five oxygen atoms, resulting in the creation of an oxygen vacancy (Fig. 10d) and increasing the oxygen content chemisorbed on the surface of the catalyst, which is conducive to the adsorption of C_3H_8 and the activation of the C-H bond, and effectively improves the catalytic oxidation performance. These enhancements are directly evidenced by the significantly improved propane conversion over P-doped $LaCoO_3$ (Fig. 10e).

View Article Online
DOI: 10.1039/D5NR01880C

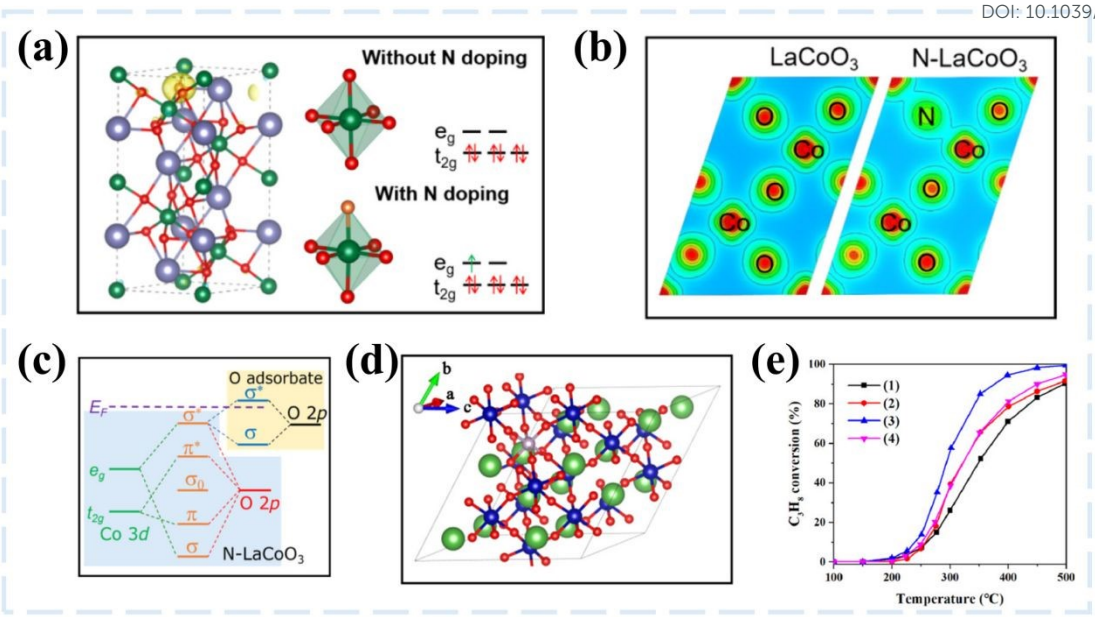

Fig. 10. (a) Spin density distribution and electronic configuration of $LaCoO_3$ and N-doped $LaCoO_3$. **(b)** Two-dimensional projected charge density distribution diagrams of $LaCoO_3$ and N-doped $LaCoO_3$. **(c)** Schematic diagram of orbital bonding. **(d)** Most stable structure for P-doped $LaCoO_3$ with one oxygen vacancy.[98] **(e)** C_3H_8 conversion as a function of reaction temperature.[79]

4.1.3 A-Site and B-Site Co-doping

As long as the perovskite structure is acceptable in the range of atomic radii (tolerance factor t of 0.75-1.00), all elements can be doped to the original perovskite. The A and B sites of the perovskite structure were partially replaced with different elements at the same time, resulting in a simultaneously doped perovskite oxide ($A_{1-x}A'_xB_{1-y}B'_yO_3$) with elements at the A and B sites. The A-site doping charge is not conserved, creating many unsaturated bonds, and the d-orbital electrons of the B-site ions must be altered in order to maintain the stability and electroneutrality of the system. B-site doping increases the electron leaving domains, reduces the localized peaks,

View Article Online
DOI: 10.1039/D5NR01880C

decreases the intensity of O, and increases the p-orbital range of O. The p-orbitals of O overlap to a greater extent with the d-orbitals of the B-site elements. The interaction of the B-site and O produces a stable octahedral structure. LM-based perovskite catalysts were modified by A and B sites.[99] Sr replaces the A site in LM, reducing the intensity of the d-orbital peaks and the degree of interatomic electronic hybridization of La, which in turn reduces the interaction between O and La in perovskite, leading to a portion of the O being uncoordinated with La and the formation of oxygen-deficient crystal cells. Doping K in LSM weakens the s-electron leaving domain of O and reduces its bonding ability. The interactions between O and Sr and O and La are weakened, the bonding capacity is low, and oxygen-deficient crystal cells are easily formed. After the perovskite structure is doped with Sr and K ions, the charge in the system becomes non-conservative and many unsaturated coordination bonds are formed. In order to keep the system stable and remain electrically neutral, the d-orbital electrons of Mn must be changed. The Mn-O bonds become weaker, the intensity and overlap of the Mn-O peaks are reduced, and the lattice oxygen in the system is susceptible to migration, which leads to the creation of oxygen defective units and oxygen vacancies in the system. Orbital electron hybridization between Mn and O promotes the general stability of the perovskite catalyst and maintains the stability of the overall catalytic system. The partial substitution of Cu for the Mn site increases the electronic leaving domains, lowers the local peaks, reduces the intensity of O and strengthens the bonding with Cu, and also increases the p-orbital range of O. The p-orbitals of O overlap the d-orbitals of Mn and Cu, respectively (Fig. 11a-d). This interaction between Mn, O and Cu produces stable

View Article Online
DOI: 10.1039/D5NR01880C

octahedral structures. In conclusion, the addition of Sr, K and Cu to LM perovskite can change the way atoms interact in the system, resulting in oxygen-deficient crystal cells, which improves the activity and stability of the catalyst.

The A-site cation indirectly affects the electronic structure of the B-site ion, leading to a change in the B-O bond length of the B-site ion, as well as altering the number of oxygen vacancies within the catalyst. In addition, simultaneous doping of the A-site and B-site can simultaneously achieve the modulation of the structural and electronic properties of the perovskite catalysts, thus effectively increasing the active oxygen density and redox capacity of the catalyst materials and maximizing the catalytic activity of the catalysts. The perovskite $La_{1-x}Ce_xMn_{1-y}Ni_yO_3$ was doped with Ce and Ne and then used for the catalytic combustion of toluene.[80] The doped Ni ions in perovskite not only increased the Mn^{4+} content and adjusted the structural defects to maintain the charge balance, but also reduced the distortion of Mn^{4+} in perovskite. With more oxygen vacancies generated by doping Ce and Ni elements, gas-phase oxygen is continuously adsorbed into the oxygen vacancies, accepting electrons to form molecularly adsorbed oxygen, which is further converted into reactive adsorbed oxygen and lattice oxygen, promoting the continuous oxidation of toluene (Fig. 11e). In addition, there are perovskites of Sr, Fe co-doped $La_{1-x}Sr_xCo_{1-y}Fe_yO_3$ (x = 0, 0.3, 0.5,0.8; y = 0, 0.2, 0.5) for catalytic combustion of toluene.[18] The doping of Sr enhances the covalency of the B-O bond, which makes the perovskite lattice appear to have a greater degree of overlap between the 3d orbitals of the B-site and the 2p orbitals of the O-site, which leads to a decrease in the formation energy of the oxygen vacancies, and so is

View Article Online
DOI: 10.1039/D5NR01880C

more conducive to the generation of oxygen vacancies. Fe doping on the B-site optimizes the concentration of Co^{4+} and the reduction of Co^{4+}/Co^{3+} is accompanied by the formation of oxygen vacancies, while Fe doping on the B-site allows perovskite to maintain its structural stability under high temperature reaction. The synergistic effect of Sr/Fe co-doping can increase the surface adsorbed oxygen and promote the internal lattice oxygen migration to the surface, which further improves the generation of oxygen vacancies and the mobility of lattice oxygen (Fig. 11f), thus enhancing the perovskite catalytic activity.

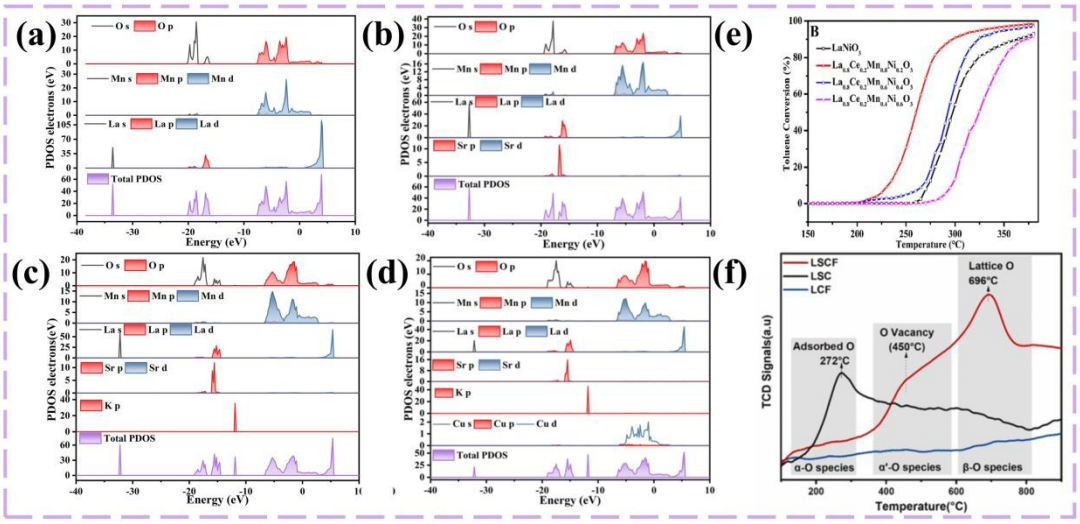

Fig. 11. (a-d) LM, LSM, $LSK_{0.12}M$, $LSK_{0.12}MCu_{0.1}$ catalysts PDOS atlas and valence electron calculated geometries.[99] **(e)** The catalytic activity of $LaNiO_3$ and $La_{0.8}Ce_{0.2}Mn_{1-y}Ni_yO_3$ (y = 0.2, 0.4, 0.6).[80] **(f)** O_2-TPD profiles of LSCF, LCF, and LSC catalysts.[18]

4.1.4 O-site doping

In recent years, the modification of perovskite for anionic O-site doping has attracted more and more research discussions. Anions such as S^{2-},[100] Cl^-,[101] and F^- [102]

View Article Online
DOI: 10.1039/D5NR01880C

can be doped into the O sites of perovskite oxides (Fig. 12a-c). Anion doping modulates the properties of perovskite oxides by replacing lattice oxygen or occupying oxygen vacancies into oxygen sites, or anions occupying interlayer gaps in the crystal structure, using valence equilibrium, electronegativity, and energy band structure, and has a significant effect on perovskite's electronic structure, chemical stability, metal-oxygen bonding strength, crystal structure, thermal expansion, electrical conductivity, and oxygen vacancy concentration. Anion doping regulates oxygen vacancies more flexibly than metal ion doping.[103]

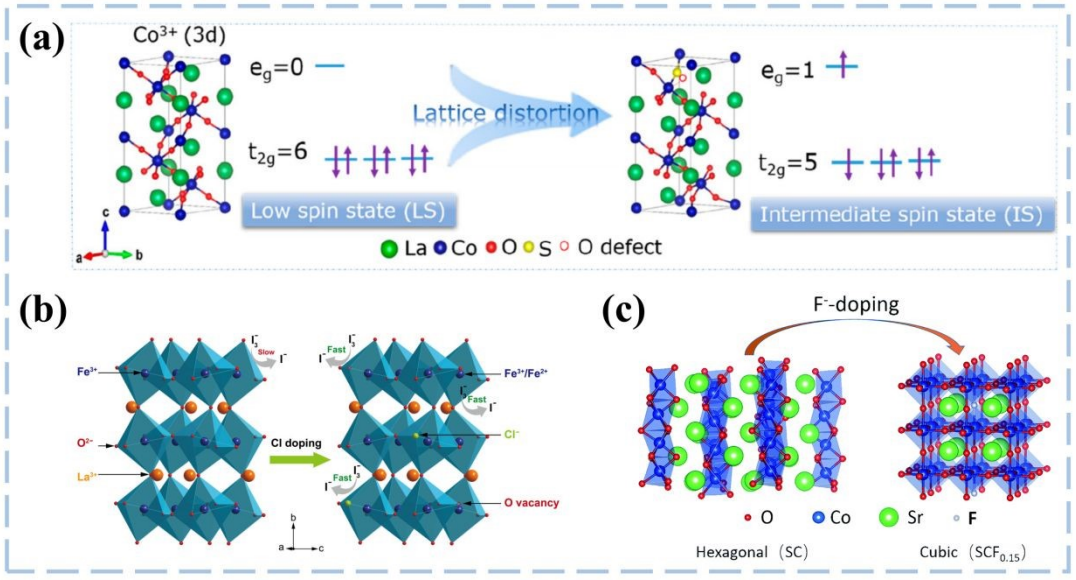

Fig. 12. (a) Sulfur-doped perovskites.[100] **(b)** Chlorine-doped perovskites.[101] **(c)** Fluorine-doped perovskites.[102]

When anions are introduced into the perovskite lattice, it leads to changes in the structural regularity and stability of the crystal. In general, the lattice parameter and cell volume of perovskite decrease with increasing anion doping. When F is doped into the lattice sites, it leads to lattice contraction because its ionic radius is smaller than O^{2-}.[104]

View Article Online
DOI: 10.1039/D5NR01880C

Doping of elements such as Cl, Br, N and S can lead to lattice expansion to a certain extent because the ionic radius is larger than O^{2-}. In this case, lattice distortion occurs due to changes in the electronic structure.[103] The effect of anion doping on the oxygen vacancy concentration depends mainly on the doping route. When halide ions directly replace lattice oxygen, the oxidation state of nearby metal cations is subsequently reduced in order to maintain electrical neutrality in the system, making lattice oxygen more susceptible to loss while increasing oxygen vacancy concentrations. When anions displace oxygen vacancies or interlayer gaps in the crystal structure, the resulting decrease in concentration is noticeable if they displace oxygen vacancies, and the introduction of anions into interlayer gaps also follows the principle of electroneutrality, leading to an increase in the oxidation state of the neighboring cations. Instead, in this case, lattice oxygen becomes less likely to be lost, leading to an overall decrease in oxygen vacancy concentration.[103,105] For anion doping with higher electronegativity than oxygen, this doped anion has a strong electron-withdrawing effect, which can reduce the valence electron density of oxygen when it occupies the O-site of the lattice, leading to a weakening of the Coulombic force between the B-site ions and the oxygen ions, a weakening of the B-O hybridization, and a weakening of the bonding interactions between O and B. In addition, the activation energy required for oxygen ion dissociation is reduced; oxygen vacancies are more readily formed; while oxygen ion mobility is improved.[103,106] Doping with anions less electronegative than O increases the valence electron density of oxygen, theoretically leading to an increase in covalency between metal and oxygen.[107-110]

View Article Online
DOI: 10.1039/D5NR01880C

Among them, F-doping has been studied more extensively than other types of anionic doping. The main reason for this is that F is the only element with a stronger electronegativity than O, plus it has a smaller ionic radius than the oxygen ion. Therefore, F doping has significant advantages over other types of anionic doping in terms of tuning oxygen vacancies and promoting oxygen ion migration.[103] Li et al. used a hydrothermal method combined with thermal calcination to construct the catalyst $LaCoO_3$, which was then doped with fluorine into perovskite and applied to the catalytic combustion of toluene (Fig. 13a).[81] Based on the electronegativity characteristics of F (3.98), La (1.1) and Co (1.9), the Co-F bond should be weaker than the La-F bond. In LCO, most of the F ions preferentially bind to La ions rather than Co ions. This promotes the presence of more La ions in the native body, which in turn triggers a decrease in the surface La/Co ratio. Ultimately, exposure to the active Co substance is significantly increased as a result. Because surface Co^{3+} species act as active sites in the catalytic oxidation of hydrocarbons, and abundant Co^{3+} species can promote the adsorption and activation of hydrocarbons, more Co^{3+} exposure on the catalyst surface enhances the adsorption and activation of toluene molecules (Fig. 13c-e).[83,111,112] At the same time, more electron-deficient Co^{3+} would have facilitated the charge transfer from the toluene molecule to the catalyst surface, making the interaction between the toluene molecule and the F-substituted LCO stronger (Fig. 13b). The high electrophilicity of F leads to a lower electron density and weaker Co-O bond strength around the lattice oxygen, which results in an easier release of O_{latt} from the surface and a lower formation energy of oxygen vacancies.

View Article Online
DOI: 10.1039/D5NR01880C

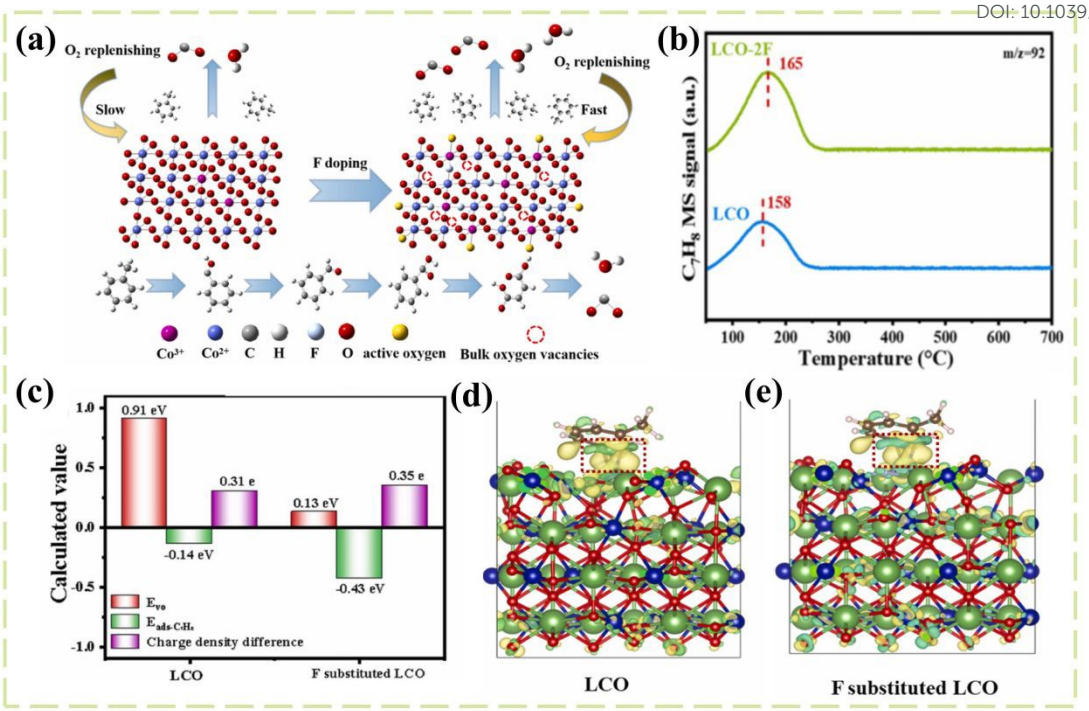

Fig. 13. (a) The proposed toluene degradation mechanism over LCO and LCO-2F. **(b)** The desorption behavior of toluene in LCO and LCO-2F as a function of temperature. **(c)** The adsorption energy of toluene over LCO and F substituted LCO. **(d-e)** The electron transfer between toluene and the LCO surface.[81]

4.2 Surface modifications

Acid, base and salt treatments can improve the surface properties of perovskite and enhance catalytic activity. Perovskites typically have a low surface area and the natural surface is preferentially occupied by A-site cations, which are not catalytically active. If the A-site cation can be selectively removed from ABO_3, the active B-site cation will be retained.[113] For ABO_3 perovskites, individual A-O bonds are typically longer than B-O bonds and have higher surface energies, which theoretically offers the possibility of selectively removing A-site cations from the perovskite backbone.[82,113,114]

View Article Online
DOI: 10.1039/D5NR01880C

In the case of acid treatment, for example, the shortening of the B-O bond length and the increase in the degree of octahedral distortion after acid etching lead to a change in the local coordination environment. Acid etching produces small concentrations of A-site deficiencies, and deletion of the A-site has a significant effect on the regulation of the valence of the B-site and the nature of the oxygen ligand.[115] A-site defects may cause a net charge imbalance in perovskite systems. The missing positive charge can be directly compensated by cations and oxygen vacancies in the B-site to balance the overall charge neutrality. Compensating for the electrons released during the formation of oxygen vacancies reduces the energy barrier for vacancy formation.[116] Electronic modulation leads to an increase in the valence of the B-site cation and the introduction of ligand holes. A slight increase in the valence state of the B-site cation is observed after acid etching. Increasing the oxidation state of the B-site cation can be thought of as reducing the number of d electrons and increasing the electronegativity of the metal ion due to the reduced electron shielding. The d-band of the B-site cation overlaps more with the s and p orbitals of oxygen, which leads to enhanced lattice oxygen activity. In a typical MvK mechanism, surface lattice oxygen species are involved in multiphase catalytic reactions. Molecular O_2 can be adsorbed and activated on oxygen vacancies, and then reactive oxygen can be readily transferred to replenish depleted surface lattice oxygen. The B-O covalency is enhanced and the antibonding state exhibits a larger oxygen signature, which enhances the adsorption capacity.[117,118] Enhanced hybridization of B-O bonds after acid etching. Hybridization of the d orbitals of B with the O 2p orbitals after acid etching brings the center of the d band closer to the Fermi

View Article Online
DOI: 10.1039/D5NR01880C

energy level, reduces the charge transfer energy and enhances the electron transport efficiency.[118]

Treatment with acids, bases and salts increases the specific surface area of the catalyst, etches the pores to increase porosity and removes the A-site ions to expose the active sites, leading to an increased likelihood of interactions with reactants and, most importantly, an increase in the amount and mobility of surface oxygen.[115,119] $LaFeO_3$ perovskite can be surface modified by etching with nitric acid for different times.[82] It was found that the acid preferentially dissolved the La cations on the $LaFeO_3$ surface, altering the La/Fe ratio, while the perovskite phase was unchanged, so that more Fe-O terminals were exposed on the catalyst surface. The best performance was obtained for the samples treated with one hour of surface etching, suggesting that the proper surface reconstruction induced by the acid treatment promotes the formation of more active Fe sites on the surface and lowers the energy barrier for methane activation. Nitric acid treatment improves catalytic activity compared to virgin LFO catalysts (Fig. 14a-b). In addition, treatment of $La_{0.8}Sr_{0.2}CoO_3$ with dilute oxalic acid selectively removes some of the Sr cations and slightly reduces the LSCO surface, leading to an increase in the amount of Co^{2+} and Lewis acid sites, which facilitates the activation of lattice and adsorbed oxygen species and promotes propane adsorption and dissociation (Figure 14c-d).[83] Rod $MnO_2/LaMnO_3$ catalysts were treated with alkaline hydrothermal and acid etching for the catalytic combustion of toluene.[84] The alkaline hydrothermal method transformed the morphology of $LaMnO_3$ from bulk to rod-like and enhanced the porous structure by selectively dissolving the A-site (La cation) in the subsequent

View Article Online
DOI: 10.1039/D5NR01880C

acid etching treatment (Fig. 14e-g). The increase in the surface Mn^{4+} / Mn^{3+} ratio after acid-etch treatment significantly improves the low-temperature catalytic activity and exhibits low apparent activation energy (Fig. 14h). In addition, alkaline-acid treatment increased the concentration of lattice oxygen on the catalyst surface and produced a high oxygen vacancy density (Fig. 14i), which promoted the redox cycling of the MvK mechanism in the catalytic oxidation reaction, which facilitated the adsorption and subsequent oxidation of toluene.

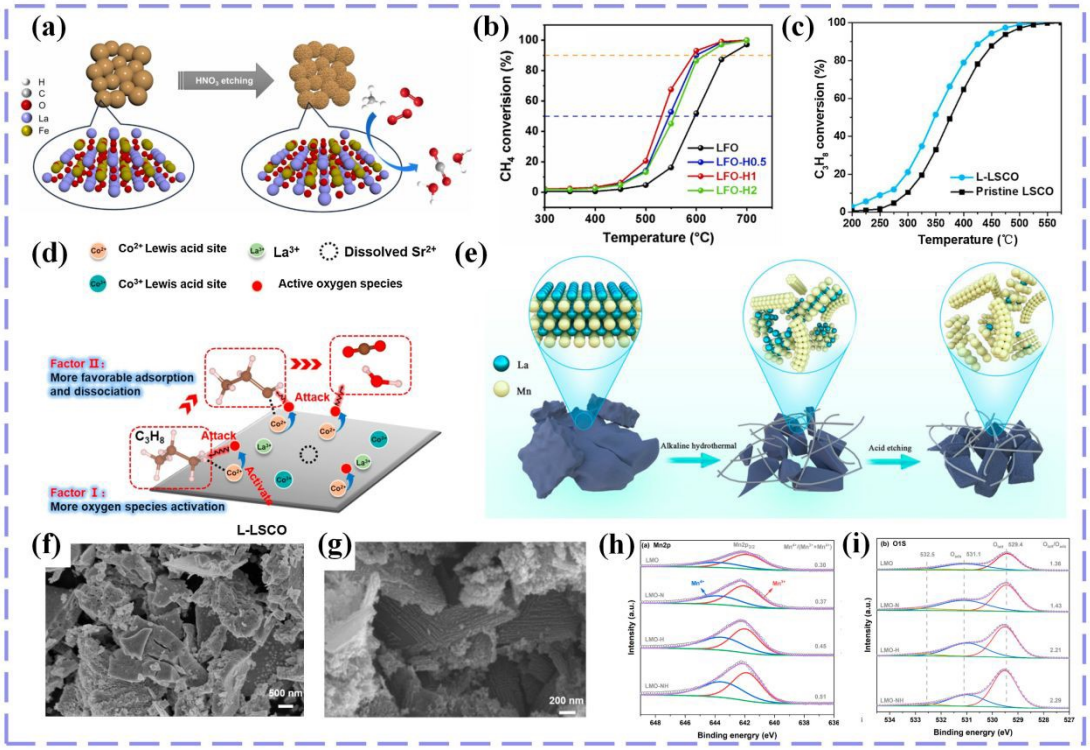

Fig. 14. (a) Nitric acid etching treatment to modify $LaFeO_3$ surface. **(b)** Catalytic activity of CH_4 combustion over pristine LFO and LFO-Hx after acid treatment.[82] **(c)** Light-off curves for propane oxidation over Pristine LSCO and L-LSCO. **(d)** Schematic explanation of superior surface reactivity on L-LSCO.[83] **(e)** Synthesis Path and Morphologic Transformation of LMO-NH. SEM patterns of **(f)** LMO and **(g)** LMO-

View Article Online
DOI: 10.1039/D5NR01880C

NH. XPS profiles of the obtained LMO samples: **(h)** Mn 2p and **(i)** O 1s.[84]

5. Conclusions and prospect

Perovskite materials (ABO_3) exhibit unique advantages in the field of catalytic combustion of volatile organic pollutants (VOCs) by virtue of their tunable lattice oxygen activity, flexible electronic structure, and diverse redox properties. By systematically resolving the enhancement mechanisms of doping modification (elemental substitution at A/B/O sites), surface reconstruction (acid-base etching) and other strategies, the relationship between the electronic structure parameters (degree of filling of e_g orbitals, the position of d-band center, concentration of oxygen vacancies, charge-transfer barriers, and degree of hybridization of the d-p orbitals, etc) and the catalytic performance has been elucidated. The electronic structure of perovskite catalysts determines their VOC catalytic combustion performance: (1) Cation defects (such as A-site vacancies) can optimize the covalent nature of B-O bonds and the occupation of e_g orbitals, thus enhancing charge mobility and activating O_{latt} near defects; (2) B-site elements with an occupancy number close to 1 are conducive to O_2 adsorption/activation, accelerating the oxidation kinetics of VOCs; (3) The multiple energy levels of d-orbitals in B-site transition metals impart complex band structures with multiple bands and gaps in perovskites, which govern VOC adsorption capacity and electron-hole recombination rates in catalysts; (4) The oxygen vacancy concentration is directly related to the generation of reactive oxygen species, promoting the MvK cycle. These structure-activity relationships provide a theoretical basis for the rational design of high-performance perovskites.

View Article Online
DOI: 10.1039/D5NR01880C

However, most of the existing studies focus on the correlation between static electronic states and macroscopic properties, while there is still a lack of systematic knowledge on the dynamic evolution mechanism of electronic structure, multi-component synergism and industrial scenario suitability under complex reaction conditions. In order to make the leap from laboratory research to industrial-scale VOCs purification technology, there is an urgent need to launch a multi-dimensional attack on the following key scientific issues and technical challenges:

(1) Novel material design and multi-dimensional regulation strategies

More targeted electronic structure modulation methods need to be developed in the future: ①Artificial Intelligence is being applied to discover new perovskite-type crystal structures and predict the component-electronic state-activity conformational relationships of perovskites, reducing the cost and cycle time of development while achieving multi-parameter optimization of catalyst preparation processes;[120-122] ② Exploring multi-scale synergistic regulation—for example, dynamic optimization of electronic states through core-shell structures, heterogeneous interfaces or surface modifications (e.g. oxygen vacancy gradient distribution);[123-125] ③ Development of flexible perovskite materials, the use of stress, light or electric fields and other external field coupling effects to dynamically regulate the electronic energy band structure, to achieve "on-demand response" intelligent catalysis.[126,127]

(2) In-depth analysis of the dynamic catalytic mechanism

Existing studies are mostly based on static characterization, while the mechanism of the dynamic evolution of the electronic structure under real reaction conditions is not

View Article Online
DOI: 10.1039/D5NR01880C

yet clear. The future can be aided by: ① Combining DFT calculations with a variety of in-situ physical and chemical characterization techniques is becoming essential. These techniques include in situ infrared and Raman spectroscopy, in situ XPS, XRD, XAS, and transmission electron microscopy. By employing these methods, it is possible to follow the electron transfer paths in perovskite oxides before and after catalytic testing;[128,129] ② Spatio-temporal correlation between electronic excited states on catalyst surfaces and molecular activation of VOCs by ultrafast spectroscopic techniques;[130] ③ Multi-scale theoretical simulations (DFT + Dynamical Monte Carlo) reveal the law of the influence of electronic structure fluctuations on the reaction energy barrier. This will provide a theoretical basis for the construction of dynamic electron regulation models.[131-133]

(3) Improvement of antitoxicity and long-lasting stability of complex systems

Competitive multi-component adsorption, water vapor interference and chlorine poisoning in real industrial exhaust gases pose challenges to the stability of the electronic structure of perovskite catalysts. Future research should focus on: ① Designing perovskite systems with self-healing capabilities, e.g., maintaining electronic structure stability through reversible oxygen vacancy migration;[134,135] ② d-Orbital modification is an effective strategy for developing new perovskites. The development of perovskites with higher low-temperature deep oxidation activity and inhibition of toxic by-products was achieved by investigating the relationship between different d-orbital filled electronic states of the catalysts and toxic by-products.[136,137]

(4) Technological breakthroughs in engineering applications

View Article Online
DOI: 10.1039/D5NR01880C

Practical applications need to be addressed: ① The problem of controlling the homogeneity of electronic structure in large-scale preparation, and the development of precise preparation techniques such as atomic layer deposition and microfluidic synthesis;[138-141] ② Development of modular catalyst carriers for high dispersion anchoring of active components through surface electronic state modulation;[142-144] ③ Establishment of a whole life cycle evaluation system and development of a strategy for the regeneration and utilization of perovskite catalysts in conjunction with the concept of circular economy.[145,146]

(5) New perovskite electronic structure control technology – plasma

Plasma is a partially ionized gas, consisting of excited and ionized free electrons, ions, radicals and neutral species.[147] On one hand, the active species generated by the plasma can directly react with VOC molecules, oxidizing and decomposing them. On the other hand, these active species can also activate the surface of the perovskite catalyst, enhancing the catalyst's ability to adsorb and oxidize VOCs, thus significantly improving the overall removal efficiency of VOCs.[148] Currently, plasma is mostly used to assist in the catalytic oxidation of VOCs. There have been few reports on the impact of plasma technology on the electronic structure of perovskite, so future research should focus on: ① Modelling the structure-property relationship between plasma parameters (power, atmosphere, pulse frequency) and perovskite electronic structure;[149,150] ② Coupled in situ plasma-XAS/XPS technique to analyze the dynamic evolution of the d-band center and oxygen vacancy concentration under reaction conditions;[148,151,152] ③ Develop plasma coupling technology to achieve electronic gradient design of core-shell

View Article Online
DOI: 10.1039/D5NR01880C

structure perovskite, improving adaptability to complex flue gas.[153,154]

Declaration of Competing Interest

The authors declare that they have no known competing financial interests or personal relationships that could have appeared to influence the work reported in this paper.

Data Availability

No primary research results, software or code have been included and no new data were generated or analysed as part of this review.

Acknowledgments

This work was supported by the Projects of the Science and Technology Department of Sichuan Province (2023NSFSC0841), the Sichuan University Postdoctoral Interdisciplinary Innovation Fund (JCXK2208), and the Fundamental Research Funds for the Central Universities (2023SCU12099).

References

1 F. I. Khan and A. Kr. Ghoshal, *J. Loss Prev. Process Ind.*, 2000, **13**(6), 527-545. DOI: https://doi.org/10.1016/S0950-4230(00)00007-3.

2 W. B. Li, J. X. Wang and H. Gong, *Catal. Today*, 2009, **148**(1), 81-87. DOI: https://doi.org/10.1016/j.cattod.2009.03.007.

3 T. Masui, H. Imadzu, N. Matsuyama and N. Imanaka, *J. Hazard. Mater.*, 2010, **176**(1), 1106-1109. DOI: https://doi.org/10.1016/j.jhazmat.2009.11.108.

4 M. S. Kamal, S. A. Razzak and M. M. Hossain, *Atmos. Environ.*, 2016, **140**, 117-134. DOI: https://doi.org/10.1016/j.atmosenv.2016.05.031.

5 L. F. Liotta, *Appl. Catal. B Environ.*, 2010, **100**(3), 403-412. DOI: https://doi.org/10.1016/j.apcatb.2010.08.023.

6 M. Zimowska, A. Michalik-Zym, R. Janik, T. Machej, J. Gurgul, R. P. Socha, J. Podobiński and E. M. Serwicka, *Catal. Today*, 2007, **119**(1), 321-326. DOI: https://doi.org/10.1016/j.cattod.2006.08.022.

7 W. Tang, G. Liu, D. Li, H. Liu, X. Wu, N. Han and Y. Chen, *Sci China Chem.*, 2015, **58**(9), 1359-1366. DOI: 10.1007/s11426-015-5469-8.

8 X. Chen, S. A. C. Carabineiro, S. S. T. Bastos, P. B. Tavares, J. J. M. órfão, M. F. R. Pereira and J. L. Figueiredo, *J. Environ. Chem. Eng.*, 2013, **1**(4), 795-804. DOI: https://doi.org/10.1016/j.jece.2013.07.019.

9 M. A. Peña and J. L. G. Fierro, *Chem. Rev.*, 2001, **101**(7), 1981-2018. DOI: 10.1021/cr980129f.

10 Y. Liu, W. Wang, X. Xu, J. Marcel Veder and Z. Shao, *J. Mater. Chem. A*, 2019, **7**(13), 7280-7300. DOI: 10.1039/C8TA09913H.

11 M. Risch, *Catalysts*, 2017, **7**(5), 154. DOI: 10.3390/catal7050154.

12 A. M. Manjón-Sanz, T. W. Surta, P. Mandal, A. J. Corkett, H. Niu, E. Nishibori, M. Takata, J. B. Claridge and M. J. Rosseinsky, *Chem. Mat.*, 2022, **34**(1), 29-42. DOI: 10.1021/acs.chemmater.1c01979.

13 A. Paul, I. Dasgupta and S. Bandyopadhyay, *Phys. Rev. B*, 2020, **101**(1), 14109. DOI: 10.1103/PhysRevB.101.014109.

14 Z. Pan, J. Chen, R. Yu, H. Yamamoto, Y. Rong, L. Hu, Q. Li, K. Lin, L. You, K. Zhao, L. Fan, Y. Ren, K. Kato, M. Azuma and X. Xing, *Inorg. Chem.*, 2016, **55**(19), 9513-9516. DOI: 10.1021/acs.inorgchem.6b01661.

15 L. C. C. B. Oliveira, R. Venâncio, P. V. F. De Azevedo, C. G. Anchieta, T. C. M. Nepel, C. B. Rodella, H. Zanin and G. Doubek, *J. Energy Chem.*, 2023, **81**, 1-19. DOI: https://doi.org/10.1016/j.jechem.2023.02.013.

16 A. R. Gandhe, J. S. Rebello, J. L. Figueiredo and J. B. Fernandes, *Appl. Catal. B Environ.*, 2007, **72**(1), 129-135. DOI: https://doi.org/10.1016/j.apcatb.2006.10.017.

17 S. Ordóñez, L. Bello, H. Sastre, R. Rosal and F. V. Díez, *Appl. Catal. B Environ.*, 2002, **38**(2), 139-149. DOI: https://doi.org/10.1016/S0926-

View Article Online
DOI: 10.1039/D5NR01880C

3373(02)00036-X.

18 Y. Li, S. Liu, K. Yin, D. Jia, Y. Sun, X. Zhang, J. Yan and L. Yang, *J. Environ. Chem. Eng.*, 2023, **11**(1), 109050. DOI: https://doi.org/10.1016/j.jece.2022.109050.

19 K. Everaert and J. Baeyens, *J. Hazard. Mater.*, 2004, **109**(1), 113-139. DOI: https://doi.org/10.1016/j.jhazmat.2004.03.019.

20 X. Li, X. Li, X. Zeng and T. Zhu, *Appl. Catal. Gen.*, 2019, **572**, 61-70. DOI: https://doi.org/10.1016/j.apcata.2018.12.026.

21 D. R. Jones and T. G. G. Maffeïs, *Sens. Actuators. B. Chem.*, 2015, **218**, 16-24. DOI: https://doi.org/10.1016/j.snb.2015.04.072.

22 P. Wang, L. Wang, Y. Zhao, B. Zhang and D. Wang, *Water Air Soil Poll.*, 2023, **235**(1), 7. DOI: 10.1007/s11270-023-06802-x.

23 S. Zhao, Y. Wang, Y. Zhang, J. Bai, Y. Zhang, S. Wang and E. Duan, *Fuel*, 2023, **345**, 128258. DOI: https://doi.org/10.1016/j.fuel.2023.128258.

24 T. Wang, J. Wang, Y. Sun, Y. Duan, S. Sun, X. Hu, S. Xi, Y. Du, C. Wang and Z. J. Xu, *Appl. Catal. B Environ.*, 2019, **256**, 117844. DOI: https://doi.org/10.1016/j.apcatb.2019.117844.

25 H. Gao, Z. Song, Y. Mao, Y. Fan, R. Li, X. Chen, W. Liu, J. Zhang, Z. Huang and X. Zhang, *Appl. Catal. B Environ Energy*, 2025, **362**, 124745. DOI: https://doi.org/10.1016/j.apcatb.2024.124745.

26 P. Liu, Y. Liao, J. Li, L. Chen, M. Fu, P. Wu, R. Zhu, X. Liang, T. Wu and D. Ye, *J. Colloid. Interface. Sci.*, 2021, **594**, 713-726. DOI: https://doi.org/10.1016/j.jcis.2021.03.093.

27 Q. Fu, S. Wang, T. Wang, D. Xing, X. Yue, M. Wang and S. Wang, *J. Catal.*, 2022, **405**, 129-139. DOI: https://doi.org/10.1016/j.jcat.2021.11.014.

28 J. Suntivich, H. A. Gasteiger, N. Yabuuchi, H. Nakanishi, J. B. Goodenough and Y. Shao-Horn, *Nat. Chem.*, 2011, **3**(7), 546-550. DOI: 10.1038/nchem.1069.

29 Y. Qiu, R. Gao, W. Yang, L. Huang, Q. Mao, J. Yang, L. Sun, Z. Hu and X.

Liu, *Chem. Mat.*, 2020, **32**(5), 1864-1875. DOI: 10.1021/acs.chemmater.9b04287.

30 D. Du, R. Zheng, M. He, C. Zhao, B. Zhou, R. Li, H. Xu, X. Wen, T. Zeng and C. Shu, *Energy Storage Mater.*, 2021, **43**, 293-304. DOI: https://doi.org/10.1016/j.ensm.2021.09.011.

31 F. Liu, Z. Zhang, L. Shi, Y. Zhang, X. Qiu, Y. Dong, H. Jiang, Y. Zhu and J. Zhu, *J. Mater. Chem. A*, 2023, **11**(20), 10596-10604. DOI: 10.1039/D3TA01063E.

32 Z. Zhu, M. Zhou, Z. Fan, Q. Wu, K. Tan, Y. Liu, Y. Chen and J. Liu, *ACS Appl. Energ. Mater.*, 2023, **6**(10), 5155-5166. DOI: 10.1021/acsaem.3c00014.

33 G. Assat and J. Tarascon, *Nat. Energy*, 2018, **3**(5), 373-386. DOI: 10.1038/s41560-018-0097-0.

34 J. Greeley, F. Studt, J. Rossmeisl, T. R. Munter, P. G. Moses, E. Skúlason, T. Bligaard, J. K. Nørskov and F. Abild-Pedersen, *Phys. Rev. Lett.*, 2007, **99**(1), 16105. DOI: 10.1103/PhysRevLett.99.016105.

35 Y. Xu, J. Dhainaut, J. Dacquin, J. Lamonier, H. Zhang and S. Royer, *Appl. Catal. B Environ.*, 2024, **342**, 123400. DOI: https://doi.org/10.1016/j.apcatb.2023.123400.

36 Y. Zhu, W. Zhou, J. Yu, Y. Chen, M. Liu and Z. Shao, *Chem. Mat.*, 2016, **28**(6), 1691-1697. DOI: 10.1021/acs.chemmater.5b04457.

37 Z. Su, J. Wu, T. Song, L. Duan, P. Zhang, L. Sun and K. Fan, *J. Mater. Chem. A*, 2025, **13**(4), 2789-2800. DOI: 10.1039/D4TA07345B.

38 Y. Xu, J. Dhainaut, J. Dacquin, J. Lamonier, H. Zhang and S. Royer, *Appl. Catal. B Environ.*, 2024, **342**, 123400. DOI: https://doi.org/10.1016/j.apcatb.2023.123400.

39 X. Liu, J. Mi, L. Shi, H. Liu, J. Liu, Y. Ding, J. Shi, M. He, Z. Wang, S. Xiong, Q. Zhang, Y. Liu, Z. Wu, J. Chen and J. Li, *Angew Chem Int Edit.*, 2021, **60**(51), 26747-26754. DOI: https://doi.org/10.1002/anie.202111610.

40 L. Tang, Z. Chen, F. Zuo, B. Hua, H. Zhou, M. Li, J. Li and Y. Sun, *Chem.*

Eng. J., 2020, **401**, 126082. DOI: https://doi.org/10.1016/j.cej.2020.126082.

41 X. Kuai, G. Yang, Y. Chen, H. Sun, J. Dai, Y. Song, R. Ran, W. Wang, W. Zhou and Z. Shao, *Adv. Energy Mater.*, 2019, **9**(38), 1902384. DOI: https://doi.org/10.1002/aenm.201902384.

42 P. Wu, X. Jin, Y. Qiu and D. Ye, *Environ. Sci. Technol.*, 2021, **55**(8), 4268-4286. DOI: 10.1021/acs.est.0c08179.

43 J. Zhu, H. Li, L. Zhong, P. Xiao, X. Xu, X. Yang, Z. Zhao and J. Li, *ACS Catal.*, 2014, **4**(9), 2917-2940. DOI: 10.1021/cs500606g.

44 J. Hwang, R. R. Rao, L. Giordano, K. Akkiraju, X. R. Wang, E. J. Crumlin, H. Bluhm and Y. Shao-Horn, *Nat. Catal.*, 2021, **4**(8), 663-673. DOI: 10.1038/s41929-021-00656-4.

45 L. Giordano, K. Akkiraju, R. Jacobs, D. Vivona, D. Morgan and Y. Shao-Horn, *Acc. Chem. Res.*, 2022, **55**(3), 298-308. DOI: 10.1021/acs.accounts.1c00509.

46 C. Shang, X. Xiao and Q. Xu, *Coord. Chem. Rev.*, 2023, **485**, 215109. DOI: https://doi.org/10.1016/j.ccr.2023.215109.

47 H. Falcón, J. A. Barbero, J. A. Alonso, M. J. Martínez-Lope and J. L. G. Fierro, *Chem. Mat.*, 2002, **14**(5), 2325-2333. DOI: 10.1021/cm011292l.

48 R. M. García De La Cruz, H. Falcón, M. A. Peña and J. L. G. Fierro, *Appl. Catal. B Environ.*, 2001, **33**(1), 45-55. DOI: https://doi.org/10.1016/S0926-3373(01)00157-6.

49 M. Christy, S. Choi, J. Kwon, J. Jeong, U. Paik and T. Song, *Small. Sci.*, 2025, **5**(1), 2400386. DOI: https://doi.org/10.1002/smsc.202400386.

50 L. Yang, Y. Li, Y. Sun, W. Wang and Z. Shao, *Energy Environ. Mater.*, 2022, **5**(3), 751-776. DOI: https://doi.org/10.1002/eem2.12256.

51 L. Xiang, L. Zhang, J. Shao, F. Lin, Z. Wang, B. Yan and G. Chen, *J. Hazard. Mater.*, 2023, **441**, 129997. DOI: https://doi.org/10.1016/j.jhazmat.2022.129997.

52 N. Guo, Z. Wang, C. Yuan, Z. Wang, L. Jiang, Q. Wang, Z. Du and Y. Liu, *Sep. Purif. Technol.*, 2025, **353**, 128296. DOI:

https://doi.org/10.1016/j.seppur.2024.128296.

53 S. Wu, G. Wu, P. Wang and G. Guo, *Int. J. Hydrog. Energy.*, 2023, **48**(27), 10288-10298. DOI: https://doi.org/10.1016/j.ijhydene.2022.12.149.

54 Y. J. Kim, D. Kim, Y. Kim, Y. Jeong, B. Jeong and J. Y. Park, *Int. J. Mol. Sci.*, 2023, **24**(1), 810. DOI: 10.3390/ijms24010810.

55 A. Kachmar, G. Berdiyorov and M. E. Madjet, *J. Phys. Chem. C.*, 2019, **123**(7), 4056-4063. DOI: 10.1021/acs.jpcc.8b11651.

56 Y. Gao, D. Lin, P. Liu, T. Shi and W. Xie, *Mater. Chem. Front.*, 2024, **8**(3), 785-799. DOI: 10.1039/D3QM00969F.

57 L. Zhao, L. Jiang, Y. Huang, J. Zhang, J. Tang and C. Li, *Appl. Surf. Sci.*, 2022, **578**, 151977. DOI: https://doi.org/10.1016/j.apsusc.2021.151977.

58 M. A. Haque, A. Syed, F. H. Akhtar, R. Shevate, S. Singh, K. Peinemann, D. Baran and T. Wu, *ACS Appl. Mater. Interfaces*, 2019, **11**(33), 29821-29829. DOI: 10.1021/acsami.9b07751.

59 F. Lin, Z. Zhang, N. Li, B. Yan, C. He, Z. Hao and G. Chen, *Chem. Eng. J.*, 2021, **404**, 126534. DOI: https://doi.org/10.1016/j.cej.2020.126534.

60 X. Weng, P. Sun, Y. Long, Q. Meng and Z. Wu, *Environ. Sci. Technol.*, 2017, **51**(14), 8057-8066. DOI: 10.1021/acs.est.6b06585.

61 H. Acosta Pérez, C. A. López, O. J. Furlong, M. S. Nazzarro, S. G. Marchetti, L. E. Cadús and F. N. Agüero, *Catalysts*, 2023, **13**(1), 42. DOI: 10.3390/catal13010042.

62 Q. Dai, K. Shen, W. Deng, Y. Cai, J. Yan, J. Wu, L. Guo, R. Liu, X. Wang and W. Zhan, *Environ. Sci. Technol.*, 2021, **55**(6), 4007-4016. DOI: 10.1021/acs.est.0c08256.

63 X. Feng, M. Tian, C. He, L. Li, J. Shi, Y. Yu and J. Cheng, *Appl. Catal. B Environ.*, 2020, **264**, 118493. DOI: https://doi.org/10.1016/j.apcatb.2019.118493.

64 C. He, J. Cheng, X. Zhang, M. Douthwaite, S. Pattisson and Z. Hao, *Chem. Rev.*, 2019, **119**(7), 4471-4568. DOI: 10.1021/acs.chemrev.8b00408.

65 S. Saha, K. Kishor and R. G. S. Pala, *Catal. Sci. Technol.*, 2024, **14**(16), 4566-4574. DOI: 10.1039/D4CY00448E.

66 X. Yu, M. Shi, Y. Fan, L. Yang, J. Zhang, W. Liu, W. Dai, S. Zhang, L. Zhou, X. Luo and S. Luo, *Appl. Catal. B Environ.*, 2022, **309**, 121236. DOI: https://doi.org/10.1016/j.apcatb.2022.121236.

67 H. Jia, Y. Xing, L. Zhang, W. Zhang, J. Wang, H. Zhang and W. Su, *Sci. Total Environ.*, 2023, **865**, 161063. DOI: https://doi.org/10.1016/j.scitotenv.2022.161063.

68 J. Geng, Q. Ke, W. Zhou, W. Wang, S. Wang, Y. Zhou and H. Lu, *J. Fuel Chem. Technol.*, 2022, **50**(5), 564-576. DOI: https://doi.org/10.1016/S1872-5813(21)60182-2.

69 C. Lv, M. Hu, T. Yuan, L. Yan and H. Chen, *Catal. Sci. Technol.*, 2022, **12**(11), 3670-3684. DOI: 10.1039/D2CY00476C.

70 E. W. Mcfarland and H. Metiu, *Chem. Rev.*, 2013, **113**(6), 4391-4427. DOI: 10.1021/cr300418s.

71 L. Wei, Z. Wang, Y. Liu, G. Guo, H. Dai, S. Cui and J. Deng, *J. Hazard. Mater.*, 2021, **416**, 126117. DOI: https://doi.org/10.1016/j.jhazmat.2021.126117.

72 S. Royer, A. Van Neste, R. Davidson, S. Mcintyre and S. Kaliaguine, *Ind. Eng. Chem. Res.*, 2004, **43**(18), 5670-5680. DOI: 10.1021/ie030775r.

73 M. B. Liu and B. Yildiz, *Chem. Mat.*, 2024, **36**(21), 10571-10582. DOI: 10.1021/acs.chemmater.4c01936.

74 R. Zhang, H. Alamdari and S. Kaliaguine, *Appl. Catal. Gen.*, 2008, **340**(1), 140-151. DOI: https://doi.org/10.1016/j.apcata.2008.02.028.

75 X. Xiang, L. Zhao, B. Teng, J. Lang, X. Hu, T. Li, Y. Fang, M. Luo and J. Lin, *Appl. Surf. Sci.*, 2013, **276**, 328-332. DOI: https://doi.org/10.1016/j.apsusc.2013.03.091.

76 C. Zhang, W. Hua, C. Wang, Y. Guo, Y. Guo, G. Lu, A. Baylet and A. Giroir-Fendler, *Appl. Catal. B Environ.*, 2013, **134-135**, 310-315. DOI:

https://doi.org/10.1016/j.apcatb.2013.01.031.

77 S. Qi, W. Zhang, X. Li, Q. Wang, Z. Zhu, T. Zhou, G. Wang, A. Xie and S. Luo, *Environ. Prog. Sustain. Energy*, 2023, **42**(1), e13965. DOI: https://doi.org/10.1002/ep.13965.

78 C. Zhang, C. Wang, W. Zhan, Y. Guo, Y. Guo, G. Lu, A. Baylet and A. Giroir-Fendler, *Appl. Catal. B Environ.*, 2013, **129**, 509-516. DOI: https://doi.org/10.1016/j.apcatb.2012.09.056.

79 Y. Luo, Y. Zheng, X. Feng, D. Lin, Q. Qian, X. Wang, Y. Zhang, Q. Chen and X. Zhang, *ACS Appl. Mater. Interfaces*, 2020, **12**(21), 23789-23799. DOI: 10.1021/acsami.0c01599.

80 B. Yuan, Y. Tao, S. Qi, A. Xie and S. Luo, *Environ. Sci. Pollut. Res.*, 2023, **30**(13), 36993-37003. DOI: 10.1007/s11356-022-24916-3.

81 B. Li, H. Xiong, W. Dai, Z. Huang, X. Zhong, J. Zhang, L. Zhou, K. Wu, J. Zou and X. Luo, *Appl. Catal. B Environ Energy*, 2024, **347**, 123828. DOI: https://doi.org/10.1016/j.apcatb.2024.123828.

82 X. Wu, M. Li, A. Abouserie, A. Frommelius, G. Dalfollo, T. Ohlerth and U. Simon, *Catal. Today*, 2024, **432**, 114620. DOI: https://doi.org/10.1016/j.cattod.2024.114620.

83 J. Yang, L. Shi, L. Li, Y. Fang, C. Pan, Y. Zhu, Z. Liang, S. Hoang, Z. Li and Y. Guo, *Catal. Today*, 2021, **376**, 168-176. DOI: https://doi.org/10.1016/j.cattod.2020.06.043.

84 S. Wang, Q. Liu, Z. Zhao, C. Fan, X. Chen, G. Xu, M. Wu, J. Chen and J. Li, *Ind. Eng. Chem. Res.*, 2020, **59**(14), 6556-6564. DOI: 10.1021/acs.iecr.0c00373.

85 H. Wang, W. Xu, S. Richins, K. Liaw, L. Yan, M. Zhou and H. Luo, *Electrochim. Acta.*, 2019, **296**, 945-953. DOI: https://doi.org/10.1016/j.electacta.2018.11.075.

86 J. Suntivich, H. A. Gasteiger, N. Yabuuchi, H. Nakanishi, J. B. Goodenough and Y. Shao-Horn, *Nat. Chem.*, 2011, **3**(7), 546-550. DOI:

View Article Online
DOI: 10.1039/D5NR01880C

10.1038/nchem.1069.

87 W. Rahim, A. Cheng, C. Lyu, T. Shi, Z. Wang, D. O. Scanlon and R. G. Palgrave, *Chem. Mat.*, 2020, **32**(22), 9573-9583. DOI: 10.1021/acs.chemmater.0c02806.

88 X. Cheng, E. Fabbri, M. Nachtegaal, I. E. Castelli, M. El Kazzi, R. Haumont, N. Marzari and T. J. Schmidt, *Chem. Mat.*, 2015, **27**(22), 7662-7672. DOI: 10.1021/acs.chemmater.5b03138.

89 Z. Shi, J. Guo, Y. Chen, Q. Li, Y. Pan, H. Zhang, Y. Xia and W. Huang, *Adv. Mater.*, 2017, **29**(16). DOI: 10.1002/adma.201605005.

90 L. Guo, L. Bo, Y. Li, Z. Jiang, Y. Tian and X. Li, *Solid State Sci.*, 2021, **113**, 106519. DOI: https://doi.org/10.1016/j.solidstatesciences.2020.106519.

91 X. Lincheng, W. Yue, Y. Yong, H. Zhanzhong, C. Xin and L. Fan, *Appl. Energy.*, 2023, **339**, 120931. DOI: https://doi.org/10.1016/j.apenergy.2023.120931.

92 B. Chen, C. Wang, F. Xue, J. Bi, M. Xia, M. Cui, Y. Pan, Z. Fei and X. Qiao, *Catal. Lett.*, 2024, **154**(6), 2878-2890. DOI: 10.1007/s10562-023-04504-x.

93 G. Tang, Z. Xiao and J. Hong, *J. Phys. Chem. Lett.*, 2019, **10**(21), 6688-6694. DOI: 10.1021/acs.jpclett.9b02530.

94 T. Tang, X. Bai, X. Xu, Z. Wang and J. Guan, *J. Colloid. Interface. Sci.*, 2025, **680**, 676-683. DOI: https://doi.org/10.1016/j.jcis.2024.11.029.

95 Y. Liang, F. Li, X. Cui, C. Stampfl, S. P. Ringer, X. Yang, J. Huang and R. Zheng, *Sci. Adv.*, **11**(11), eads7054. DOI: 10.1126/sciadv.ads7054.

96 J. Ding, L. Zhao, Y. Yang and J. Liu, *J. Mater. Chem. A*, 2025, **13**(10), 7371-7380. DOI: 10.1039/D4TA06446A.

97 Y. Liu, H. Huang, L. Xue, J. Sun, X. Wang, P. Xiong and J. Zhu, *Nanoscale*, 2021, **13**(47), 19840-19856. DOI: 10.1039/D1NR05797A.

98 B. Xia, T. Wang, J. Ran, S. Jiang, X. Gao and D. Gao, *ACS Appl. Mater. Interfaces*, 2021, **13**(2), 2447-2454. DOI: 10.1021/acsami.0c16150.

99 C. Li, W. Dai, Z. Li, R. Niu, Q. Guo, H. Qiao, P. Liu and C. Zhang, *Mol.*

Catal., 2024, **559**, 114085. DOI: https://doi.org/10.1016/j.mcat.2024.114085.

100 J. Ran, T. Wang, J. Zhang, Y. Liu, C. Xu, S. Xi and D. Gao, *Chem. Mat.*, 2020, **32**(8), 3439-3446. DOI: 10.1021/acs.chemmater.9b05148.

101 W. Wang, R. Tran, J. Qu, Y. Liu, C. Chen, M. Xu, Y. Chen, S. P. Ong, L. Wang, W. Zhou and Z. Shao, *ACS Appl. Mater. Interfaces*, 2019, **11**(39), 35641-35652. DOI: 10.1021/acsami.9b07966.

102 W. Wang, Y. Yang, D. Huan, L. Wang, N. Shi, Y. Xie, C. Xia, R. Peng and Y. Lu, *J. Mater. Chem. A*, 2019, **7**(20), 12538-12546. DOI: 10.1039/C9TA03099A.

103 C. Yang, Y. Tian, C. Yang, G. Kim, J. Pu and B. Chi, *Adv. Sci.*, 2023, **10**(35), 2304224. DOI: https://doi.org/10.1002/advs.202304224.

104 C. C. Yang, Y. F. Tian, J. Pu and B. Chi, *ACS Sustain. Chem. Eng.*, 2022, **10**(2), 1047-1058. DOI: 10.1021/acssuschemeng.1c07576.

105 Y. Xie, N. Shi, D. M. Huan, W. Z. Tan, J. F. Zhu, X. S. Zheng, H. B. Pan, R. R. Peng and C. R. Xia, *ChemSusChem*, 2018, **11**(19), 3423-3430. DOI: 10.1002/cssc.201801193.

106 J. Xiong, H. Zhong, J. Li, X. L. Zhang, J. W. Shi, W. W. Cai, K. G. Qu, C. Z. Zhu, Z. H. Yang, S. P. Beckman and H. S. Cheng, *Appl. Catal. B Environ.*, 2019, **256**. DOI: 10.1016/j.apcatb.2019.117817.

107 R. Li, J. Long, M. Li, D. Du, L. Ren, B. Zhou, C. Zhao, H. Xu, X. Wen, T. Zeng and C. Shu, *Mater. Today Chem.*, 2022, **24**, 100889. DOI: https://doi.org/10.1016/j.mtchem.2022.100889.

108 W. Qin, Z. Yuan, Y. Shen, R. Zhang and F. Meng, *Chem. Eng. J.*, 2022, **431**, 134280. DOI: https://doi.org/10.1016/j.cej.2021.134280.

109 Y. Miyahara, K. Miyazaki, T. Fukutsuka and T. Abe, *Chem. Commun.*, 2017, **53**(18), 2713-2716. DOI: 10.1039/c6cc09890h.

110 Y. L. Zhu, Q. Lin, Z. B. Wang, D. C. Qi, Y. C. Yin, Y. Liu, X. W. Zhang, Z. P. Shao and H. T. Wang, *J. Energy Chem.*, 2021, **52**, 115-120. DOI: 10.1016/j.jechem.2020.03.055.

111 C. Feng, Q. Gao, G. Xiong, Y. Chen, Y. Pan, Z. Fei, Y. Li, Y. Lu, C. Liu and Y. Liu, *Appl. Catal. B Environ.*, 2022, **304**, 121005. DOI: https://doi.org/10.1016/j.apcatb.2021.121005.

112 J. Zhong, Y. Zeng, D. Chen, S. Mo, M. Zhang, M. Fu, J. Wu, Z. Su, P. Chen and D. Ye, *J. Hazard. Mater.*, 2020, **386**, 121957. DOI: https://doi.org/10.1016/j.jhazmat.2019.121957.

113 W. Si, Y. Wang, Y. Peng and J. Li, *Angew Chem Int Edit.*, 2015, **54**(27), 7954-7957. DOI: https://doi.org/10.1002/anie.201502632.

114 H. Chen, W. Cui, D. Li, Q. Tian, J. He, Q. Liu, X. Chen, M. Cui, X. Qiao, Z. Zhang, J. Tang and Z. Fei, *Ind. Eng. Chem. Res.*, 2020, **59**(23), 10804-10812. DOI: 10.1021/acs.iecr.0c01182.

115 Q. Yang, J. Li, D. Wang, Y. Peng and Y. Ma, *Catal. Today*, 2021, **376**, 205-210. DOI: https://doi.org/10.1016/j.cattod.2020.05.056.

116 Y. Sun, H. Liao, J. Wang, B. Chen, S. Sun, S. J. H. Ong, S. Xi, C. Diao, Y. Du, J. Wang, M. B. H. Breese, S. Li, H. Zhang and Z. J. Xu, *Nat. Catal.*, 2020, **3**(7), 554-563. DOI: 10.1038/s41929-020-0465-6.

117 J. Simböck, M. Ghiasi, S. Schönebaum, U. Simon, F. M. F. de Groot and R. Palkovits, *Nat. Commun.*, 2020, **11**(1), 652. DOI: 10.1038/s41467-020-14305-0.

118 Y. Jin, W. Si, X. Yuan, H. Cheng, B. Zhou, L. Cai, Y. Wang, Q. Wang and J. Li, *Chin. Chem. Lett.*, 2025, **36**(5), 110260. DOI: https://doi.org/10.1016/j.cclet.2024.110260.

119 L. Zhao, J. Ding, J. Liu and Y. Yang, *Environ. Sci. Pollut. Res.*, 2024, **31**(1), 1456-1467. DOI: 10.1007/s11356-023-31268-z.

120 E. I. Marchenko, V. V. Korolev, E. A. Kobeleva, N. A. Belich, N. N. Udalova, N. N. Eremin, E. A. Goodilin and A. B. Tarasov, *Nanoscale*, 2025, **17**(5), 2742-2752. DOI: 10.1039/D4NR04531A.

121 J. I. Gómez Peralta and X. Bokhimi, *J. Solid State Chem.*, 2020, **285**, 121253. DOI: https://doi.org/10.1016/j.jssc.2020.121253.

122 S. Touati, A. Benghia, Z. Hebboul, I. K. Lefkaier, M. B. Kanoun and S. Goumri-Said, *Neural Comput. Appl.*, 2024, **36**(26), 16319-16329. DOI: 10.1007/s00521-024-09992-5.

123 C. Han, L. Yan, W. Zhao and Z. Liu, *Int. J. Hydrog. Energy*, 2017, **42**(17), 12276-12283. DOI: https://doi.org/10.1016/j.ijhydene.2017.03.068.

124 H. Tong, F. Li, M. Du, H. Song, B. Han, G. Jia, X. Xu, X. Zou, L. Ji, J. Kai, Z. Hu and H. Hsu, *ACS Appl. Mater. Interfaces*, 2025, **17**(16), 23431-23465. DOI: 10.1021/acsami.4c20972.

125 J. Yang, S. Hu, L. Shi, S. Hoang, W. Yang, Y. Fang, Z. Liang, C. Pan, Y. Zhu, L. Li, J. Wu, J. Hu and Y. Guo, *Environ. Sci. Technol.*, 2021, **55**(13), 9243-9254. DOI: 10.1021/acs.est.1c00511.

126 C. Zhang, S. Yuan, Y. Lou, H. Okada and Z. Wang, *Small*, 2022, **18**(16), 2107556. DOI: https://doi.org/10.1002/smll.202107556.

127 M. Zhou, J. Liu, Y. Ye, X. Sun, H. Chen, D. Zhou, Y. Yin, N. Zhang, Y. Ling, F. Ciucci and Y. Chen, *Small*, 2021, **17**(45), 2104144. DOI: https://doi.org/10.1002/smll.202104144.

128 A. L. Fernandes Cauduro, E. Gager, K. A. King, D. Mccord, A. H. Mcdaniel, J. Scheffe, J. C. Nino and F. El Gabaly, *Top. Catal.*, 2024, **67**(13), 900-908. DOI: 10.1007/s11244-024-01940-w.

129 K. Akkiraju, R. Rao, J. Hwang, L. Giordano, X. Renshaw Wang, E. Crumlin, D. S. Weinberger and Y. Shao-Horn, *ACS Catal.*, 2024, **14**(10), 7649-7663. DOI: 10.1021/acscatal.4c01222.

130 R. R. Tamming, J. M. Hodgkiss and K. And Chen, *Adv. Phys. X*, 2022, **7**(1), 2065218. DOI: 10.1080/23746149.2022.2065218.

131 J. Wang and G. Wang, *J. Phys. Chem. C*, 2024, **128**(31), 12978-12986. DOI: 10.1021/acs.jpcc.4c02579.

132 J. A. Budagosky and A. García-Cristóbal, *Nanomaterials*, 2022, **12**(17), 3052. DOI: 10.3390/nano12173052.

133 Q. Liu, A. Li, W. Chu, O. V. Prezhdo and W. Liang, *J. Mater. Chem. A*, 2022,

View Article Online
DOI: 10.1039/D5NR01880C

10(1), 234-244. DOI: 10.1039/D1TA09027E.

134 R. M. Ragin and V. Meenu, *Mater. Lett.*, 2024, **354**, 135365. DOI: https://doi.org/10.1016/j.matlet.2023.135365.

135 Y. Yu, F. Zhang and H. Yu, *Sol. Energy*, 2020, **209**, 408-414. DOI: https://doi.org/10.1016/j.solener.2020.09.018.

136 L. Ding, B. Fan, N. Fang, S. Wu, J. Li and Y. Chu, *Appl. Catal. B Environ Energy*, 2025, **366**, 125036. DOI: https://doi.org/10.1016/j.apcatb.2025.125036.

137 X. Liu, Y. Shi, L. Yu, G. Zhan, Z. Chen, B. Zhou, H. Zhang, H. Li, X. Liu, L. Zhang and Z. Ai, *Appl. Catal. B Environ Energy*, 2025, **371**, 125245. DOI: https://doi.org/10.1016/j.apcatb.2025.125245.

138 H. H. Sønsteby, H. Fjellvåg and O. Nilsen, *Adv. Mater. Interfaces*, 2017, **4**(8), 1600903. DOI: https://doi.org/10.1002/admi.201600903.

139 S. Jeon, J. Seo, J. W. Shin, S. Lee, H. G. Seo, S. Lee, N. Tsvetkov, J. Kim, J. An and W. Jung, *Chem. Eng. J.*, 2023, **455**, 140611. DOI: https://doi.org/10.1016/j.cej.2022.140611.

140 W. Lai, C. Wu and X. Han, *Chem. Eng. J.*, 2023, **451**, 138383. DOI: https://doi.org/10.1016/j.cej.2022.138383.

141 X. Liu, Y. Shi, L. Yu, B. Zhou, Z. Chen, F. Guo, H. Li, X. Liu, L. Zhang and Z. Ai, *Environ. Sci. Technol.*, 2025, **59**(12), 6331-6340. DOI: 10.1021/acs.est.4c14734.

142 Y. Cho, G. Han, S. S. Han, M. Seo and K. Lee, *Mol. Catal.*, 2020, **484**, 110732. DOI: https://doi.org/10.1016/j.mcat.2019.110732.

143 Y. Wang, S. Liu, C. Pei, Q. Fu, Z. Zhao, R. Mu and J. Gong, *Chem. Sci.*, 2019, **10**(45), 10531-10536. DOI: 10.1039/C9SC03119G.

144 Y. Wang, T. Shi, Q. Fan, Y. Liu, A. Zhang, Z. Li, Y. Hao, L. Chen, F. Liu, X. Gu and S. Zeng, *ACS Catal.*, 2022, **12**(14), 8386-8403. DOI: 10.1021/acscatal.2c01364.

145 R. G. Charles, A. Doolin, R. García-Rodríguez, K. V. Villalobos and M. L.

Davies, *Energy Environ. Sci.*, 2023, **16**(9), 3711-3733. DOI: 10.1039/D3EE00841J.

146 X. Tian, S. D. Stranks and F. You, *Nat. Sustain.*, 2021, **4**(9), 821-829. DOI: 10.1038/s41893-021-00737-z.

147 Z. Wang, Y. Zhang, E. C. Neyts, X. Cao, X. Zhang, B. W. L. Jang and C. Liu, *ACS Catal.*, 2018, **8**(3), 2093-2110. DOI: 10.1021/acscatal.7b03723.

148 K. Wu, Y. Sun, J. Liu, J. Xiong, J. Wu, J. Zhang, M. Fu, L. Chen, H. Huang and D. Ye, *J. Hazard. Mater.*, 2021, **405**, 124156. DOI: https://doi.org/10.1016/j.jhazmat.2020.124156.

149 Q. Tian, Z. Wang, M. Yuan, S. Zhao, H. Chen, L. Li, M. Cui, X. Qiao and Z. Fei, *Environ Sci-nano*, 2021, **8**(8), 2386-2395. DOI: 10.1039/D1EN00339A.

150 S. Jung and K. Chung, *Energy Conv. Manag.*, 2024, **311**, 118509. DOI: https://doi.org/10.1016/j.enconman.2024.118509.

151 B. Zhu, Q. Li, Y. Li, Y. Xia, J. Liu, A. Zhou and X. Zhang, *Chem. Eng. J.*, 2023, **469**, 143897. DOI: https://doi.org/10.1016/j.cej.2023.143897.

152 W. Feng, F. He, X. Chen, B. Jiang, H. Wang and Z. Wu, *Chem. Eng. J.*, 2024, **488**, 150804. DOI: https://doi.org/10.1016/j.cej.2024.150804.

153 W. Li, X. Liu, J. Zhang, H. Wang, C. Yuan, S. Lin, C. Chen, C. Shen, J. Tang, J. Li, T. Bu, S. Wang, Y. Jiang, X. Xiao and J. Gong, *Adv. Mater.*, 2025, **37**(12), 2417094. DOI: https://doi.org/10.1002/adma.202417094.

154 X. Yu, A. Rashid, G. Chen, M. Widenmeyer, U. Kunz, T. Shao, G. Homm, L. Molina-Luna, R. Snyders and A. Weidenkaff, *Chem. Eng. J.*, 2025, **512**, 161954. DOI: https://doi.org/10.1016/j.cej.2025.161954.

View Article Online
DOI: 10.1039/D5NR01880C

Data availability

No primary research results, software or code have been included and no new data were generated or analysed as part of this review.